On cerebral blood flow and the intracranial pressure curve

Unnerbäck, Mårten

2019

Document Version:
Publisher's PDF, also known as Version of record

[Link to publication](#)

Total number of authors:
1

$$\Delta V'_a = q_a - q_{av} + q_{reg}, \quad \Delta V'_v = q_{av} - q_v, \quad \Delta V'_c =$$

$$q_a - q_v - q_s, \quad \Delta V'_s = q_s - q_l, \quad L_s q'_s = e_c \Delta V_c -$$

$$e_s \Delta V_s - R_s$$

$$q'_{am} = q_{re}$$

$$e_v \Delta V_v),$$

On cerebral blood flow and the intracranial pressure curve

MÅRTEN UNNERBÄCK
FACULTY OF MEDICINE | LUND UNIVERSITY

$$\tau_{reg}$$

$$e_a \Delta V_a + p_c \quad , \quad p_v = e_v \Delta V_v + p_c, \; p_c = e_c \Delta V_c + p_0$$

$$p_s = e_s \Delta V_s + p_0 \; q_{reg} = \frac{(q_a - q_{am})}{\tau_{reg}}, \text{ for } V_{a0} \geqslant 0, q_{reg} =$$

$$0 \quad , \quad \text{otherwise,} \quad e_a =$$

$$e_{a0}\left(\frac{n_{e_a}}{\Delta V_a}\right)^{m_{ea}} \exp(-k_{ea}\, q_{reg}), R_{av} =$$

$$R_{av0}\left(\frac{n_{R_{av}}}{V_{a0}+\Delta V_a}\right)^{m_{Rav}} , \quad R_v = R_{v0}/\Delta V_v^{m_{Rv}} , \quad e_v =$$

$$-\frac{e_{v1}(\Delta V_v)^{m_{ev1}}}{V_{v0}+\Delta V_v}, \text{ for } \Delta V_v < 0, \; e_v = e_v, \text{ for }$$

$$\Delta V_v \geq 0, \, e_c = e_{c0} \exp(k_{ec}\, \Delta V_c), R$$

$$\text{for } q_s > 0, R_s = R_{cs}(1 - a_{R_s}), \text{ for } q_s$$

On cerebral blood flow and the intracranial pressure curve

On cerebral blood flow and the intracranial pressure curve

Mårten Unnerbäck

LUND
UNIVERSITY

DOCTORAL DISSERTATION
by due permission of the Faculty of Medicine, Lund University, Sweden.
To be defended at Föreläsningssal 1, Centralblocket, Entrégatan 7, Skåne
University Hospital, Lund, Sweden on Friday, January 11, 2019 at 09.00 a.m.

Faculty opponent
Professor Marek Czosnyka
University of Cambridge

Organization	Document name
LUND UNIVERSITY Faculty of Medicine Department of Clinical Sciences Lund Anesthesiology and Intensive Care Medicine	DOCTORAL DISSERTATION
	Date of issue January 11th, 2019
Author: Mårten Unnerbäck	Sponsoring organization

Title and subtitle: On cerebral blood flow and the intracranial pressure curve

Background: This thesis explores the physiological causes of the intracranial pressure (ICP) curve, with special emphasis on cerebral blood flow (CBF). Monitoring ICP is commonly done in neuro intensive care, in order to secure adequat CBF. What shapes the intracranial pressure curve is however not fully understood. The curve depends on the pulsatility of blood flow, and hydrodynamic causes have been suggested. If the relationship between physiology and the intracranial pressure curve is understood, analysis of the curve could provide clinical information useful in individualising treatment. The relationships can be explored measuring flow into and out from the cranial cavity in conjunction with ICP monitoring.

Methods: A database containing all patients admitted to the neuro intensive care unit in Lund and who had their CBF meausered through phase contrast MRI technology was created The database was used in order to establish relationships between the pulsatile component of the ICP curve and the pulsatile component of CBF (I), the changes in flow and intracranial volume and the ICP curve (II), the pulsatility of venous outflow from the intracranial compartment and ICP and to validate a mathehmatical model describing the intracranial hydrodynamics (IV).

Results: The area under the curve of the ICP curve correlated to pulsatile cerebral blood flow. Using elastance to calculate a volume change curve from the ICP curve strengthened the correlation (I). Comparing the ICP curve to flow and volume changes over the cardiac cycle, the initial part of the ICP curve correlated to flow changes and the latter part correlated to volume changes (II). As mean ICP increases the pulsatility of venous outflow from the cranial cavity is attenuated (III). A mathematical model based on physiological properties of the intracranial compartment can produce ICP curves in close resemblance to measured ICP curves (IV).

Conclusions: Using phase contrast MRI in conjunction with ICP monitoring it is possible to correlate the ICP curve to various features of cerebral blood flow, strengthening the hypothesis that the ICP curve is dependent on cerebral blood flow and the physiological properties of the intracranial cavity. It is possible to recreate the physiology through mathematical modeling in a way that produces ICP curves dependent on CBF.

Key words: Intracranial pressure, Cerebrovascular circulation, Phase-contrast MRI, Mathematical modeling, Hydrodynamics

Classification system and/or index terms (if any)

Recipient's notes	Number of pages FI F	Price
	Security classification	

Signature   _[signature]_   Date 2018-12-06

On cerebral blood flow and the intracranial pressure curve

Mårten Unnerbäck

LUND
UNIVERSITY

Cover photo: The mathematical model describing the hydrodynamics of the intracranial compartment.

Liseå gård, autumn 2018

To Elias, Bea and Vilgot

Table of Contents

Original papers

This thesis is based on the following four original papers, corresponding to four individual studies. They are referred to in the thesis by their Roman numerals.

I.   Unnerbäck M, Ottesen J, Reinstrup P. ICP curve morphology and intracranial flow-volume changes: a simultaneous ICP and cine phase contrast MRI study in humans. Acta Neurochirurgica (Wien); 160: 219-224. 2018.

II.   Unnerbäck M, Bloomfield E, Söderström S, Reinstrup P. The intracranial pressure curve correlates to the pulsatile component of cerebral blood flow. Journal of Clinical Monitoring and Computing; doi: 10.1007/s10877-018-0129-0. [Epub ahead of print] 2018.

III.   Unnerbäck M, Ottesen J, Reinstrup P. Increased ICP attenuates the pulsating component of cerebral venous outflow. Manuscript, submitted.

IV.   Unnerbäck M, Ottesen J, Reinstrup P. Validation of a mathematical model for understanding intracranial pressure curve morphology. Manuscript, submitted.

All published papers are reprinted with permission by the copyright owner.

Summary in Swedish

Hjärnan är vårt viktigaste organ. Den definierar om vi lever eller ej och vem vi är och den styr vår kropp, såväl medvetet som omedvetet. Lika viktig som den är för oss, lika känslig är den, ständigt beroende av en kontinuerlig tillförsel av syre och näring via blodet. Hjärnans nervceller är mycket känsliga för avbrott i denna försörjning. Inom ca 10 sekunder från att blodflödet upphör så förlorar vi medvetandet och inom minuter börjar nervcellerna ta permanent skada.

Individer som drabbas av skador i hjärnan kan behöva neurointensivvård. Denna vård riktas framför allt in på att skydda den redan skadade hjärnan mot ytterligare skada genom att säkerställa att hjärnan får det den behöver i form av syre och näring, allt för att undvika sekundära skador som kan ge patienten ytterligare skador.

Den känsliga hjärnan är omsluten av och därmed skyddad av det hårda kraniet. Detta utgör ett gott skydd mot slag och stötar, men innebär också att en svullnad, blödning eller annan form av expansion inuti kraniet kan orsaka ett ökat tryck, vilket kan motverka tillförseln av blod till hjärnan. Med ett stigande tryck intrakraniellt blir drivtrycket för hjärnans blodflöde lägre, då trycket intrakraniellt håller emot blodtrycket.

Nils Lundberg, professor i Neurokirurgi i Lund, var den förste som visade på nyttan av att mäta tryck inuti skallkaviteten kontinuerligt. Genom att föra in en tunn kateter i hjärnans vätskefyllda hålrum kunde han mäta trycket och visa hur det påverkade hur det gick för patienterna. Inom dagens neurointensivvård är detta en standardbehandling.

Om man undersöker den intrakraniella tryckkurvan registrerad hos en patient ser man att trycket varierar över hjärtcykeln. Detta beror på att blodtryck och blodflöden varierar över hjärtcykeln och på det faktum att hjärnan är omsluten av hårt ben. Detta gör att trycket stiger i början av hjärtcykeln, för att därefter falla under slutet av hjärtcykeln. Vid en närmare analys noterar man också att tryckkurvan över hjärtcykeln har flera toppar, till skillnad från blodtryckskurvan som har en eller två toppar. Detta har varit känt sedan länge och man har tidigare försökt förklara varför trycket inuti kraniet beter sig på detta vis, men utan att nå någon tydlig slutsats.

Tack vare MR-teknologi har vi idag möjlighet att mäta blodflödet till hjärnan, blodflödet från hjärnan i venerna och flödet av cerebrospinalvätska ut från och in till kraniet över en hjärtcykel. Genom att kombinera denna metod med att observera

den intrakraniella tryckkurvan kan vi undersöka hur de påverkar varandra. Om vi kan förstå hur blodflödet påverkar trycket så öppnar sig möjligheten att hos den enskilde patienten följa kliniskt viktiga parametrar genom att kontinuerligt följa hur tryckkurvan ser ut. På detta sätt skulle vi kunna individualisera behandlingen för att nå optimal effekt.

Målsättningen med avhandlingen var således att undersöka sambanden mellan blodflöden och den intrakraniella tryckkurvan.

Vi undersökte data från patienter som vårdats på neurointensivvårdsavdelningen på SUS och jämförde de blodflödesmätningar som hade gjorts med MR med de tryckkurvor som hade registrerats hos patienten samtidigt. I första studien (I) undersökte vi hur den pulserande delen av blodflödet påverkade tryckkurvan. Vi fann att det fanns en korrelation mellan dessa två och att den kunde förstärkas genom att mäta eftergivligheten intrakraniellt och applicera denna på beräkningarna.

I den andra studien (II) jämförde vi flöden och volymsförändringar intrakraniellt med tryckkurvan och kunde visa att den första delen av tryckkurvan har ett samband med snabba flödesförändringar och att den senare delen av kurvan mer påverkas av volymsförändringar.

I den tredje studien (III) ville vi undersöka om trycket intrakraniellt påverkade det venösa utflödet. Det är känt sedan tidigare att det finns ett samband mellan venöst utföde och intrakraniellt tryck över tid, men effekterna över en hjärtcykel är mindre väl undersökta. Vi kunde i denna studie visa att det venösa utflödet från hjärnan pulserar allt mindre ju högre trycket intrakraniellt är och att det därmed sannolikt finns ett samband mellan tryckkurvans form och det venösa utflödet.

I den sista studien (IV) används matematisk modellering. Vi beskriver det vi vet om cirkulationen inuti kraniet med matematiska formler och försöker därefter efterlikna uppmätta tryckkurvor. På detta sätt kunde vi visa att de många topparna på tryckkurvan sannolikt beror på tryck och volymssvängningar mellan de olika delarna av den intrakraniella cirkulationen.

Sammantaget kunde vi visa på att blodflödet till och från hjärnan påverkar trycken och att detta kan demonstreras i en matematisk modell. Med utgångspunkt från detta kan vi fortsätta att lära oss mer om sambanden och därmed i en framtid kunna nå en punkt där analys av tryckkurvan kan bidra med viktig klinisk information.

Abbreviations

ABP	Arterial blood pressure
AUC ICP	Area under curve of the ICP curve
AUC ΔV	Area under curve of the ΔV curve
AUC	Area under curve
C	Compliance
CBF	Cerebral blood flow
CBFa	Arterial inflow to the intracranial cavity
CBFv	Venous outflow from the cranial cavity
CBV	Cerebral blood volume
CBVa	Arterial cerebral blood volume
$ccCBF_{MR}$	Cardiac cycle cerebral blood flow measured with MRI
$ccCBF_{MRpuls}$	Cardiac cycle pulsatile cerebral blood flow measured with MRI
CH	Cerebellar haemorrhage
CPP	Cerebral perfusion pressure
CSF	Cerebrospinal fluid
CSFF	Cerebrospinal fluid flow into and out from the cranial cavity
E	Elastance
ECG	Electrocardiography
$Flow_{tot}$	Total flow into and out from the cranial cavity
HC	Hydrocephalus
ICA	Internal carotid artery
ICH	Intracerebral haemorrhage
ICP	Intracranial pressure
ICP_{amp}	Intracranial pressure amplitude
ICP_{max}	Maximum ICP over a cardiac cycle
ICP_{mean}	Mean intracranial pressure
ICP_{min}	Minimum ICP over a cardiac cycle
ICV	Intracranial volume
IJV	Internal jugular vein
IJV_{puls}	Pulsatile component of the flow in the IJV
$IJV_{pulsrat}$	Ratio of pulsatile flow in the IJV
k	Compartment
MAP	Mean arterial pressure
MRI	Magnetic resonance imaging

NICU	Neurosurgical intensive care unit
P	Pressure
PDMS	Patent data monitoring system
Q	Flow
R	Resistance
SAH	Subarachnoid haemorrhage
t	Time
TBI	Traumatic brain injury
V	Volume
VA	Vertebral artery
VENC	Velocity encoding
VPI	Venous pulsatile index
ΔICP	Intracranial pressure change
ΔICV	Change in intracranial volume
ΔV	Volume change
ρ	Conductance

Introduction

This thesis concerns the intracranial pressure curve and its relationship with the hydrodynamics of the intracranial cavity. The introduction provides a physiological background required to understand the theoretical reasoning concerning this relationship. It also includes a review of the methods chosen for the studies.

The intracranial volume is normally 1200-1600 ml in adults and correlates to body height[1]. The brain occupies approximately 85% of this volume, while the CSF accounts for 10% and the cerebral blood volume (CBV) constitutes 5%[2].

The brain is surrounded by the cerebrospinal fluid (CSF). Within the brain there are four ventricles communicating with each other and filled with CSF. The ventricular system allows CSF to flow into the subarachnoid space and through the foramen magnum into the spinal canal[3]. CSF is produced in the choroid plexus within the ventricular system and is absorbed through the arachnoid granulations. In the adult the CSF volume is approximately 125 – 150 ml[4] with a daily production of about 500 ml[3,5].

CSF is similar to plasma though almost protein free and with some differences in electrolyte composition. It has several functions, including homeostasis[6], buoyance, protection and transportation of waste produce from the brain[4].

The Monro-Kellie doctrine

The Monro-Kellie doctrine is of paramount importance regarding the understanding of the intracranial hydrodynamics.

The intracranial relationship between pressure and volume was first described by the Scottish anatomist Alexander Monro in 1783[7]. He observed that the brain is enclosed by the rigid cranium and that the brain itself is incompressible. Since blood also is incompressible, he concluded that the intracranial blood volume must be constant, and any arterial inflow consequently must be compensated by a venous outflow. These observations were later confirmed by George Kellie through observations during post mortal examinations and animal experiments[8]. The

doctrine was later developed by George Burrows to include cerebrospinal fluid (CSF) as one component[9].

This doctrine is today referred to as the Monro-Kellie doctrine and states that any change of one of the components must be compensated for by a reciprocal change of the others in order to keep the total volume unchanged. A consequence of this is that the introduction of a new intracranial volume, such as a haemorrhage or another type of expanding mass must be compensated by a decrease of either blood or CSF. This also applies to transient increases of mass, such as the increase of arterial cerebral blood volume due to the pulsatile cerebral blood flow.
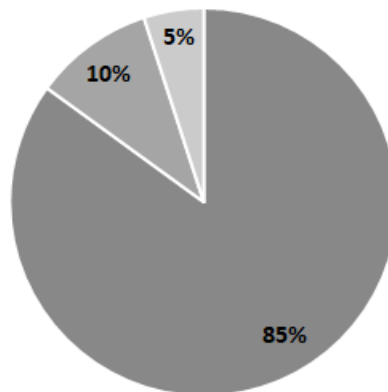
Figure 1. A schematic representation of the intracranial content
The dark grey area represents the brain, the middle grey area represents the cerebrospinal fluid volume and the light grey area represents the intracranial blood volume. The total volume is constant. If one volume is expanded or a new volume, such as a haematoma, is introduced the other volumes must decrease to compensate for this.

The intracranial pressure volume relationship

The anatomy of the cranial cavity, as enclosed in bone tissue, causes specific prerequisites regarding volume expansion and pressure.

The first measurements of pressures within the central nervous system in humans was reported by the German physician Heinrich Quincke[10], who introduced the lumbar puncture and noted increased pressure within the spinal canal in meningitis. The ventricular pressure was first measured by Hodgson in 1928[11]. Guillaume and Janny reported the first cannulations of the ventricular system in order to

continuously measure intracranial pressure (ICP) in 1951[12]. In the 1960s Nils Lundberg presented a thesis on the use of continuous ICP measurement in neurosurgical patients[13] and since then this is one of the most important tools in neuro-intensive care. The relationship between pressure and volume inside a compartment, such as the cranial cavity, can be described by using compliance (C), pressure (P) and volume (V). Any given increase in pressure induces an increase in volume and the relationship is designated as the compliance. Mathematically this is described through the equation $C = \Delta V / \Delta P$, where Δ indicate a change. If the compliance is known, this equation may be rearranged to calculate the change in volume due to a change in pressure or the change in pressure due to a change in volume, $\Delta V = C \times \Delta P$ and $\Delta P = \Delta V / C$ respectively. Another way of looking at this relationship is through elastance (E), which is defined by the equation $E = \Delta P / \Delta V$, the reciprocal of C, therefore $E = 1 / C$.

The compliance is dependent on the expandability of the compartment, exemplified by inflating a balloon, and the compressibility of the content of the compartment, as in compressing an air-filled syringe. Air is compressible at the physiological range of pressures, but solid matters and fluids are virtually incompressible at these pressures.

Since the intracranial cavity is enclosed by bone and its content is composed of fluids and solid matter, the compliance should be very low, causing a rapid increase in ICP if a change in intracranial volume occurs. However, the compliance of the intracranial cavity must be understood as a system, as it is not mainly dependent on expansion of the cavity or compression of the content but by the extrusion of content, i.e. blood and CSF. This is what Monro and Kellie observed.

As the volume inside the cranium is constant, the pressure inside the cranial cavity is dependent on the components ability to harbour an increase in one of them. If one component expands other components must be reduced by extrusion and the ICP rises to the pressure required to reach this new equilibrium. When this capacity is exhausted the intracranial pressure rises rapidly in a nonlinear manner as initially described by Ryder and colleagues[14] and through experiments determined to be of a logarithmic nature[15-17]. As the cranial cavity is connected to the spinal canal through the foramen magnum, it is more correct to use the term cranio-spinal compartment[18].
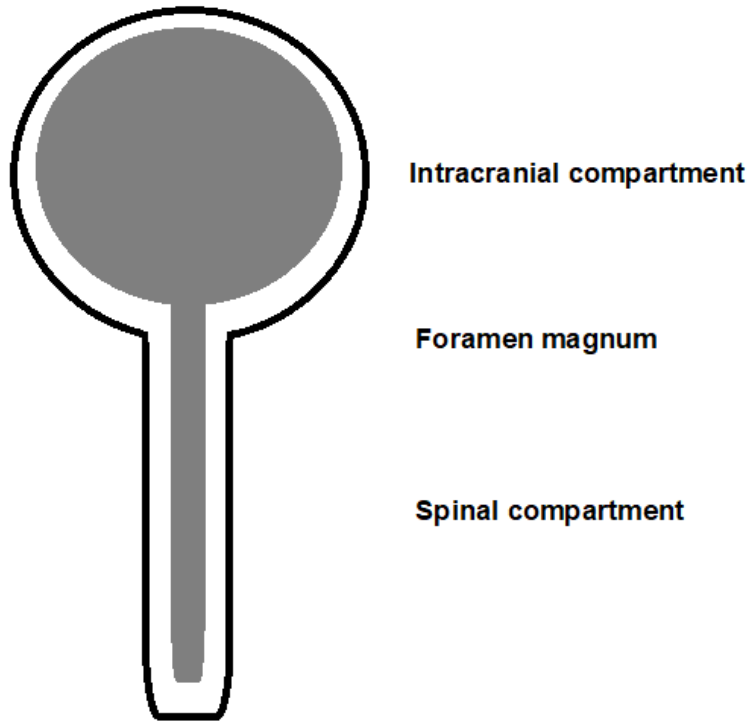
Figure 2. The cranio-spinal compartment
A schematic drawing of the cranio-spinal compartment. CSF flows between the intracranial compartment and the spinal compartment through the foramen magnum.

The relationship was experimentally determined to be a function of the natural logarithm, using elastance, in variations of the expression:

$$ICP = ICP_{eq} \times e^{E \times \Delta V},$$

where ICP_{eq} is the normal, physiological steady state ICP, before the intracranial volume change[16,19-22].

Using Magnetic Resonance Imaging (MRI) it has been shown that actually there seems to be a slight increase in intracranial volume (ICV) over the cardiac cycle due to the rapid inflow of arterial blood[23-25] and that this is compensated for in some way, possibly by movement of the brain tissue caudally[26].
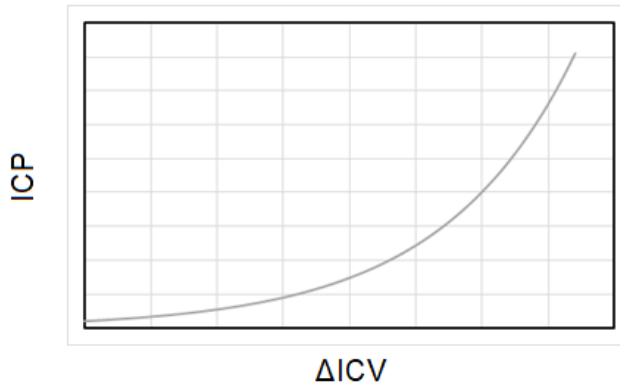
Figure 3. The cranio-spinal elastance curve
ICP as a function of ΔICV, using the cranio-spinal elastance equation. The slope of the curve is determined by the elastance.

The intracranial pressure curve morphology

The ICP varies over the cardiac cycle, producing a curve. It usually displays a number of peaks with varying amplitude. Early on these peaks were interpreted as secondary to the opening and closing of the heart valves. The peaks are named after their order, P1, P2, P3 and so on[27,28].

Another hypothesis was that the ICP curve is shaped by the transmission of the arterial blood pressure (ABP) into the cranial cavity[29]. It was noted that the ICP curve was dampened when the choroid plexuses, where arteries are in close conjunct with the ventricles, were extirpated[30]. This has however recently been questioned in a study measuring flow within the ventricular system using MRI[31].

If the transfer of the ABP is what shapes the ICP curve it is however difficult to understand the multitude of peaks featured in the ICP curve. The ABP curve is usually only composed by two peaks. To explain this, research has been conducted using Fourier transformation of the ABP curve. Since the ABP curve is composed by several sinusoidal curves the selective dampening of some of the frequencies composing the ABP curve could be the reason of the multiple peaks[32,33]. This theory does not take previous research coupling intracranial volume changes to the ICP curve into account.[19].
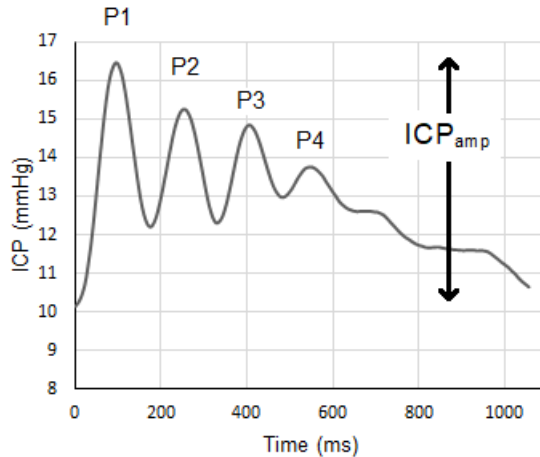
Figure 4. The intracranial pressure curve over one cardiac cycle
An intracranial pressure curve registered in one patient over one cardiac cycle. The peaks are highly distinguishable and marked P1, P2, P3 and P4. ICP$_{amp}$ is the amplitude of the curve.

Venous pulsations were also early proposed as the cause of the ICP curve[34] and in a study using dogs it was concluded that it was a combination of arterial and venous pulsations that shaped the ICP curve[35].

In an attempt to measure intracranial compliance without increasing ICP artificially by injecting fluids into the ventricular system Avezaat and colleagues began to examine the ICP amplitude. Their thought was that with every heart stroke a volume of arterial blood was injected into the intracranial cavity and thus the ICP amplitude would represent the intracranial compliance[36]. This hypothesis was tested in dogs and compared to compliance measurements by inflating a balloon intracranially. They found a linear relationship between the two models, concluding that ICP amplitude could be used to estimate elastance. They also noted that the volume-pressure relationship changed to a linear relationship when the ICP reached a certain level, which they attributed to a failure of autoregulation. They concluded that beyond this point the arterial volume injected into the cranial cavity with each heart stroke became dependent on the ICP, and therefore the calculated elastance changed[19].

By analysing the ICP curve morphology it was found that distinct features could be correlated to low cerebral blood flow[37] and intracranial compliance has been suggested to affect the ratio between P2 and P1[38]. Further measurements of ICV changes using phase contrast MRI has been linked to the ICP curve morphology[39,40].

Cerebral hydrodynamics

Cerebral blood flow

The brain is extremely vulnerable to ischemia, i.e. loss of blood supply. Within seconds of a cessation of blood supply to the brain conscience is lost[41]and within minutes the neurons start to take irreversible damage[42]. At the other extreme, if cerebral blood flow (CBF) reaches supra normal levels the brain may also be damaged due to the hyper perfusion syndrome[43].

In traumatic brain injury (TBI) secondary damage to neurons may follow the initial insult due to several mechanisms[44]. Neuro intensive care is to a large extent focused at avoiding further damage to the brain by avoiding increased ICP due to cerebral oedema formation, compromising CBF[45]. Otherwise the CBF may be insufficient to adequately oxygenate the cerebral tissue[46,47]. Bedside monitoring of CBF could possibly improve outcome in patients with head injuries[48].

Arterial blood flow

The cerebral blood flow (CBF) is supplied through four arteries, two on each side. The main supply is through the internal carotid arteries (ICA) and to a smaller extent blood is also supplied by the vertebral arteries (VA)[49].

When the heart contracts, blood flows into the cranial cavity in a pulsatile manner, i.e. it increases and decreases over the cardiac cycle. The flow is in that sense composed of a pulsatile and a constant component[50].

Measuring CBF was initially done using the Fick equation as described by Kety and Schmidt in 1944[51] and based on the arterio-venous difference in concentration of an inert freely diffusible substance, like nitrous oxide. Due to the methodology, the value of CBF is usually presented as ml/100g brain/min, where normal values are approximately 50-65 ml/100g brain/min[3]. It is not possible to determine the flow pattern over the cardiac cycle with this method and hence the ratio of pulsatile and non-pulsatile flow can´t be determined.

Another method to measure CBF is phase contrast MRI. This method measures flow in the supplying arteries over the cardiac cycle. Summarising the flow in these vessels provides the CBF over one cardiac cycle. CBF is then calculated by multiplying the flow over one cardiac cycle with the heartrate[50]. The method is reliable regarding both accuracy and reproducibility[52]. Measurements provide a flow curve over the cardiac cycle, making it possible to determine pulsatile and non-pulsatile flow.

In order to maintain blood supply to the brain the cerebral blood flow is subject to auto regulation, meaning that the CBF is kept constant within certain physiological limits and able to meet the cerebral demands. In a series of ground-breaking experiments Lassen was able to demonstrate that the CBF was consistent over a wide range of mean arterial pressure (MAP)[53].

Flow through blood vessels may be calculated by the formula $Q = \Delta P/R$, where Q is flow, ΔP is the pressure difference over the vessels and R is the resistance to blood flow through the vessels. The actual driving pressure of CBF is cerebral perfusion pressure (CPP) which is defined as $CPP = MAP - ICP$.

The autoregulation is dependent on increasing the resistance in the cerebral vascular system, thereby reducing flow[54].
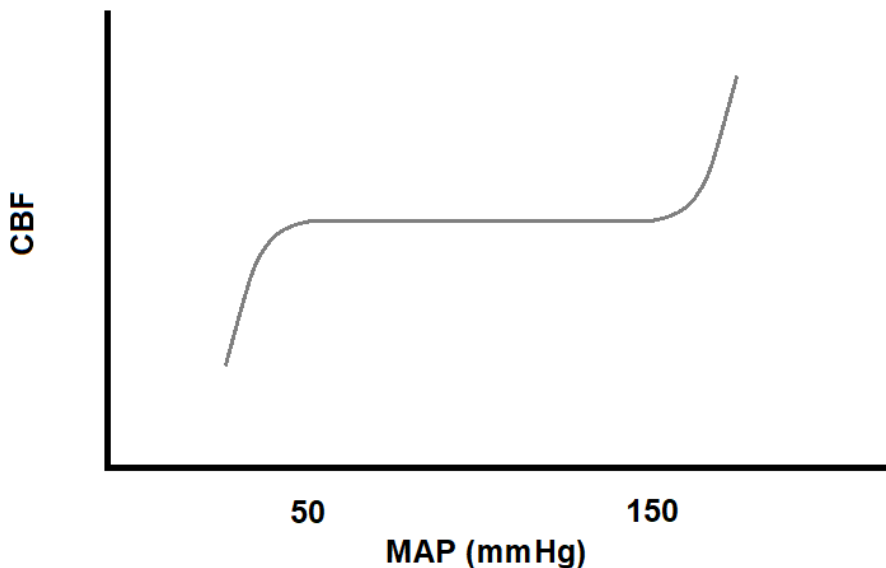
Figure 5. A representation of the Lassen curve
Cerebral blood flow as a function of the mean arterial pressure in normal conditions.

In the presence of pathological conditions, the curve may be shifted due to adaption, such as in the case of chronic hypertension[55] and there is firm evidence of dysfunction of the autoregulation in traumatic brain injury and its association with worsened outcome[56,57]. In order to maintain CBF in such circumstances, it is of value to know the individuals autoregulatory state[58,59].

Venous blood flow

Cerebral venous outflow is thought to be the result of compression of the intracerebral veins, in accordance to the Monro-Kellie doctrine. The thin walled veins are compressed by the increasing ICP and this causes expulsion of venous blood from the brain into the sinuses[26]. The venous blood flow from the cranial cavity may then take several pathways[60,61]. The principal common pathways are the internal jugular veins (IJV), whereas secondary pathways include the vertebral veins and the cervical epidural veins[61]. The meningorachidian plexus has also been suggested as an alternative pathway, depending on intrathoracic pressure or posture[62-64].

The influence of venous pressure on ICP was early recognized[34]. In cases of elevated ICP it was noted that elevating the head decreased ICP[65,66] and this has been confirmed in several studies[67-69]. Disturbances in intracranial venous outflow have been identified as a possible mechanism in intracranial pressure volume disturbances, such as idiopathic normal pressure hydrocephalus[70,71].

Cerebrospinal fluid

The flow of CSF out from the cranial cavity into the spinal canal is pulsatile and dependent on the changes in ICP over the cardiac cycle[25], dampening the ICP response to arterial intracranial inflow during systole[24]. If the communication between the intracranial cavity and the spinal canal is disturbed this capacity is reduced, causing an overall reduced compliance of the cranio-spinal system[18].

Magnetic resonance imaging

To measure the variations in CBF, cerebral venous outflow and the movement of CSF out from and into the cranial cavity over the cardiac cycle, an MRI technology was chosen.

MRI is based on the properties of protons (hydrogen atoms). The protons have the nuclear property of spin and this makes them behave like bar magnets. When placed in a magnetic field they align along the magnetic field, either with it (spin up) or against it (spin down). When aligned against the magnetic field the protons have a higher inherent energy than when they are aligned with the field. Subjected to a specific radio frequency signal some of the protons change direction from spin up to spin down. When the signal is turned off some of the protons revert to the lower energy state which causes them to emit a signal. This signal can be detected and used to produce an image of the tissue through complex signal processing[72].

Flow measurements

To measure flow through a vessel phase contrast MRI may be used. When applying brief magnetic field gradients in the direction of flow a phase shift in the magnetisation of the flowing material can be observed. This phase shift is directly proportional to the flow velocity which thereby can be calculated[73]. The flow velocity is determined in pixels and the flow of each pixel equals the area of the pixel multiplied by the flow velocity measured in that pixel. The flow in all pixels within the vessel are then summarized. If the images are acquired evenly distributed over the cardiac cycle, using gating against the ECG signal or the peripheral pulse, a flow curve over the cardiac cycle is acquired. This technique is sometimes referred to as cine phase contrast, implying the temporal component[74].
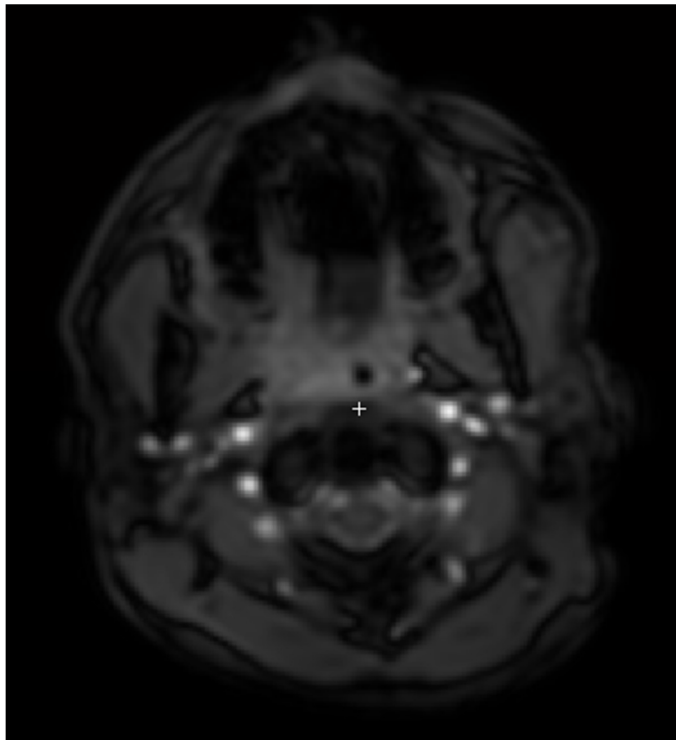
Figure 6. A scout image over the lower part of the head
The scout image is aquired perpendicular to the arteries and veins of interest. The vessels are shown bright white.

The method doesn't require calibration and has been validated against in vitro models[75,76].

The plane of the picture should be perpendicular to the flow direction to achieve optimal flow measurements, else there will be an angle dependent error underestimating flow velocity. Errors introduced by not achieving this should however mathematically be cancelled out by an increase in area of the vessel proportional to the decrease of the flow velocity.

The phase contrast images are post processed with a software which interprets the raw data and transforms the images to flow curves[77]. The areas of the vessels are encircled by a region of interest, either manually or with automated systems which differentiate flow from static tissue[78,79].
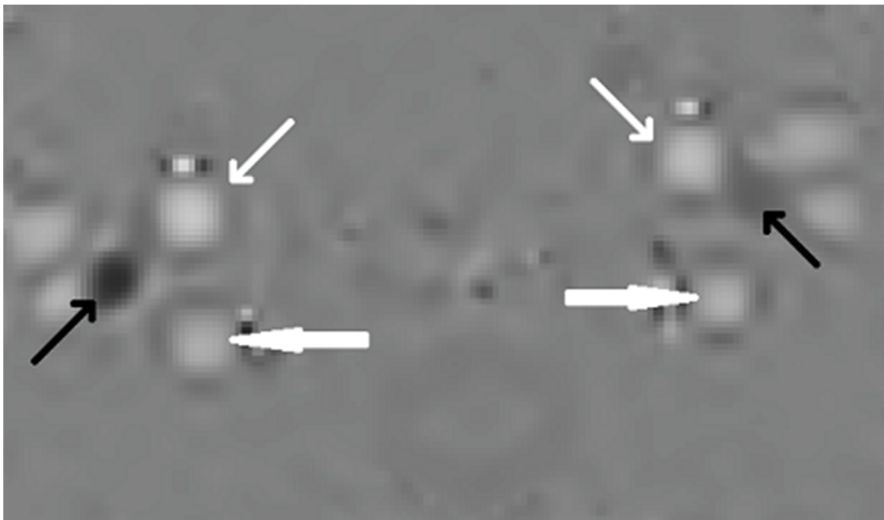
Figure 7. A phase contrast image of the vessels
One of the images of the cardiac cycle. The vessels are seen as white or black, depending on the direction of flow.
Thin white arrows represent the carotid arteries, thick white arrows the vertebral arteries and black arrows the internal jugular veins.
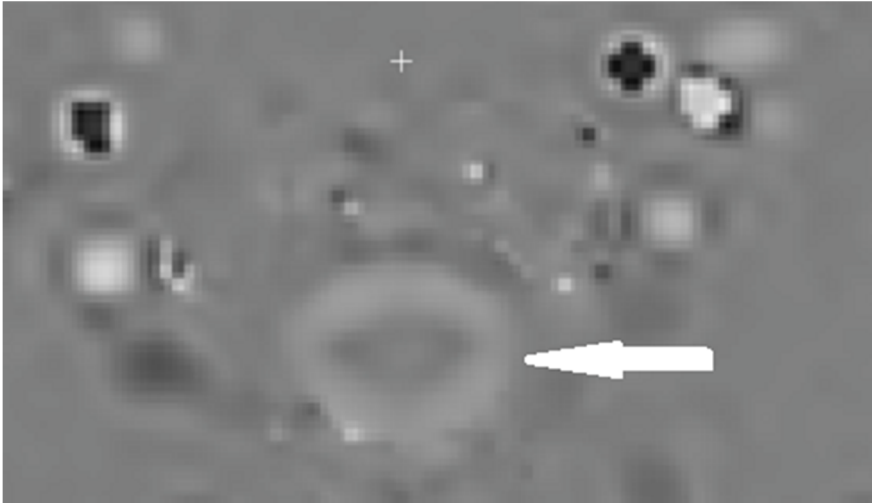
Figure 8. A phase contrast image of the cerebrospinal fluid flow
One of the images of the cardiac cycle. The CSF flow around the medulla is shown by the arrow. Aliasing phenomena can be noted in the carotid arteries in the top of the figure, due to a lower VENC used in CSF meauserments.

Possible errors of the phase contrast MRI measurement of flow include the appearance of aliasing[80]. To avoid this, the velocity encoding (VENC) has to be set above the maximum flow velocity. Setting it too high will on the other hand decrease precision. A VENC above 80 cm/s is usually sufficient to avoid this problem[74] but the maximum flow velocity in the internal carotid artery can be much higher in cases of a stenosis[81]. Aliasing is however easily detected in the images.
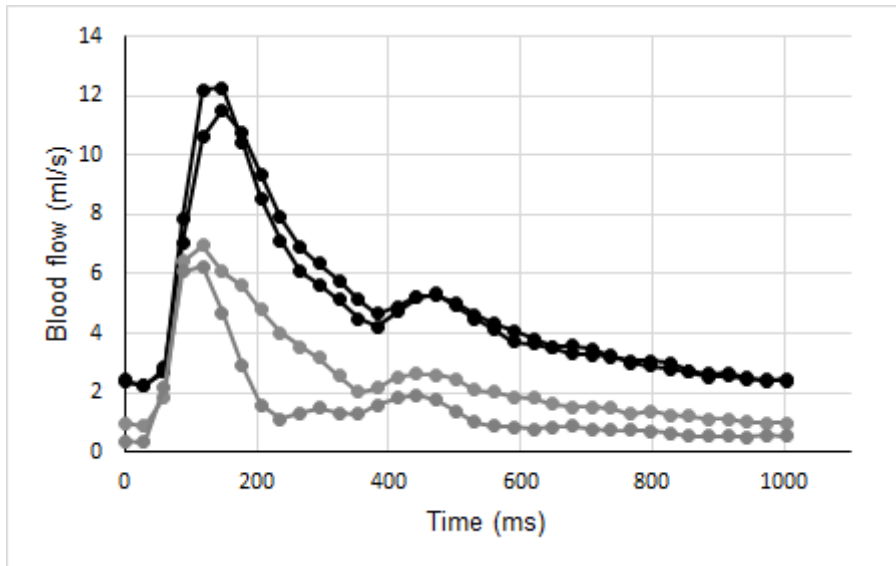
Figure 9 Arterial flow curves
The flow curves from phase contrast measurements in the internal carotid arteries in black and the vertebral arteries in grey.

The flow curves acquired with this method make it possible to analyse the relationship between the ICP curve and the flow into and out from the intracranial cavity.

Cerebral blood flow

As described above, the phase contrast technique can be used to determine CBF. By measuring the flow in the arteries supplying the brain and summarizing these flows the CBF can be calculated[50]. There have been numerous studies using this approach in healthy volunteers. The measured CBF values have been approximately 750 ml/min[24,50,52,82,83]. With an average weight of the human brain of 1200 to 1400 mg[84] this would equal approximately 55-60 ml/100g/min, compared to the 50-65 ml/100g/min derived from the techniques based on other methods[3].

Cerebral venous blood flow

Venous outflow from the cranial cavity may take several routes[60,61]. The main flow depends on the physiological state of the individual[62,63,82,85]. It is possible to measure flow in the veins draining the intracranial compartment, but in order to calculate the entire flow it must be corrected with a factor to equal arterial inflow, since all venous blood doesn't flow through the internal jugular veins[24].

CSF

CSF passes from the intracranial compartment through the foramen magnum. The flow is bidirectional, with a systolic component out from the intracranial compartment and a diastolic component where CSF flows back from the spinal compartment[86]. The flow velocity is much lower than the blood flow velocities and a lower VENC is therefore applied.
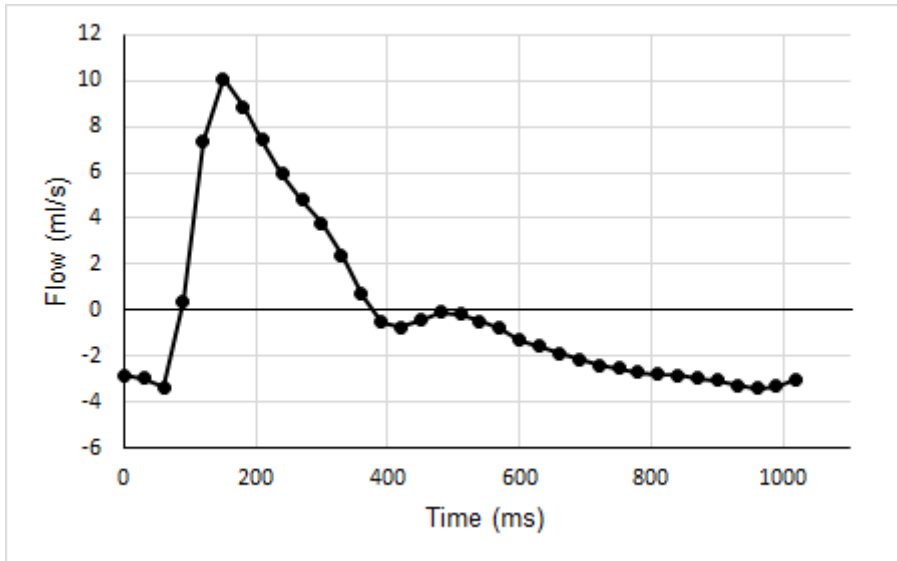
Figure 10. CSF flow curves
A flow curve from measurement of the CSF flow over the foramen magnum. Note that the flow goes from the intracranial compartment to the spinal canal (positive flow) as the arterial inflow increases and then flows back again during the latter part of the cardiac cycle (negative flow).

Intracranial volume calculation

The changes in the intracranial volumes may be calculated by using the flow of blood and CSF into and out from the cranial cavity by using the formula

$$\Delta ICV(t) = \int_{t_0}^{t} \big(CBFa(t) - CBFv(t) - CSFF(t)\big)dt$$

$\Delta ICV(t)$ is the change in intracranial volume over time. It equals the arterial, venous and CSF flow integrated over time[24]. In order to uphold the Monro-Kellie doctrine venous flow has to be corrected to equal arterial flow. These calculations have been shown to have repeatability[87].

Mathematical modelling

To further explore the hydrodynamics of the cranial cavity mathematical modelling was used.

The first description of physiology in mathematical terms was made in 1952 by Hodgkin and Huxley. It was a mathematical model of nerve excitation[88] which was later used for understanding the action and pacemaker potential in the heart by Noble[89]. Mathematical modelling has since then been used extensively to explore and understand various features of physiology[90], including circulatory and respiratory physiology[91].

The usage of mathematical models to understand and explore various features of human physiology is based on the fact that the physiology follows the rules of physics, which follow the rules of mathematics. By constructing a model based on known physiological properties of the intracranial compartment it is possible to explore the relationship between flow, volume and pressure within this compartment.

The method has previously been used to explore changes in ICP over longer periods[92,93] and to explore volumetric changes within the cranial compartment over longer time periods as well as over the cardiac cycle[94-96].

A mathematical model is either static or dynamic. In a dynamic model the results affect the calculations in the next step. As an example, an increase of pressure within a vessel increases the radius and thereby decreases the resistance to flow of that vessel. This affects the flow through the vessel and therefore affects the volume change in the next step.
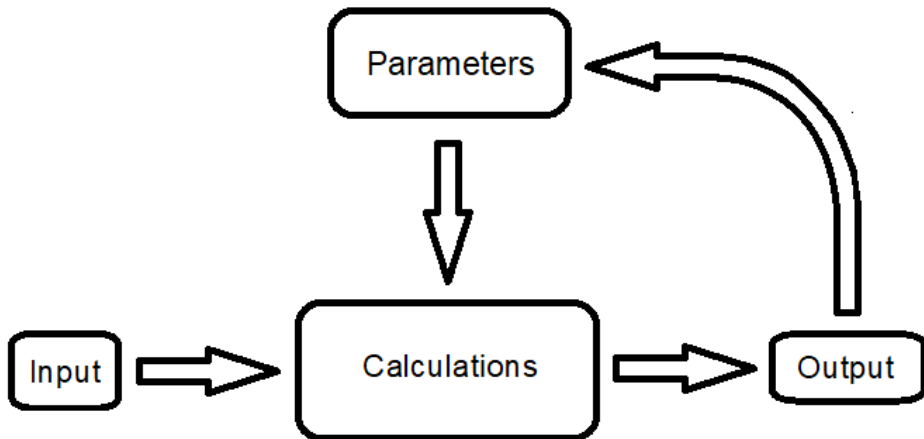
Figure 11. A dynamic mathematical model
The calculations of output data are dependent on the input and the set parameters. The output data then affects the parameters so that in the following calculations the parameters have changed, providing new output data.

Although a model is based on the physiology it represents, it is a simplification of the reality and in order to use it further it has to be validated.

Hypothesis

If the physiological causes of the ICP curve morphology are understood it may be used to analyse a patient's physiological state. Using this information may contribute to an individualised treatment.

Despite previous efforts the physiological causes of the ICP curve are still unclear[38]. The knowledge and technologies described above provide means to further the knowledge regarding the ICP curve morphology.

Aims of the thesis

The general aim of this thesis is to further the knowledge of factors causing the ICP curve morphology, especially the effect of cerebral blood flow.

The specific aims are to evaluate:

- The effect of the pulsatile arterial inflow on the ICP curve amplitude (I).
- The effect of the pulsatile arterial inflow on the ICP curve AUC (I).
- The effect on compliance on the relationship between the pulsatile arterial inflow and the ICP AUC (I)
- The relationship between intracranial volume changes and the ICP curve (II).
- The relationship between intracranial flow changes and the ICP curve (II).
- The relationship between ICP and the pulsatility of the venous outflow from the intracranial cavity (III)
- Whether an AUC technique is a comparable technique to analyse pulsatility of the intracranial venous outflow as compared to VPI (III).
- If a mathematical model, based on known physiological properties of the intracranial cavity, can mimic the ICP curve morphology from the arterial inflow curve (IV).

Methods

Ethical permission to perform the studies was sought and granted by the regional ethics committee.

Patient selection

The studies included in this thesis are based on a cohort of patients who has had their CBF measured with phase contrast MRI whilst being treated at the Neurosurgical Intensive Care Unit (NICU) at Skåne University Hospital (SUS) in Lund.

In all studies the database was searched for patients who fulfilled the criteria for each study.

Valid CBF measurements and stable ICP measurements in conjunction with the measurements were required in all studies. For paper I, an extraction of CSF in close conjunct to the CBF measurements was also required. This study also had the restriction of a time period up to the time when the study was performed (April 2013).

For paper II and IV the patients had to have their ICP measured during the MRI examination, which had been possible from May 2013. There also had to be valid phase contrast MRI measurements of CSF flow over the foramen magnum and phase contrast measurements of venous flow through the IJV. Both had to be done at the same time as the CBF measurement.

For paper III venous flow through the IJV was required at the same time as the CBF measurement.

ICP measurements

The ICP was in all patients measured with a tunnelled intraventricular catheter connected to a CSF drainage set with a pressure transducer. The reference point for the pressure transducer was the highest point of the head as per clinical practice.

Data from the pressure transducer was digitally registered through a patient monitor and stored in a database with the sampling rate of 125 Hz.

In cases where CSF had been aspirated the exact amount of CSF had been recorded in conjunction with the ICP curve at the time of extraction.

In paper I the first stable ICP curve after the MRI examination was used. Since the equation used to calculate elastance is unsolvable if the ICP goes from a negative to a positive value, the ICP was adjusted, adding 15mmHg.

In paper II and IV a composite ICP curve was used. This was calculated by adding all ICP curves over one respiratory cycle registered during the MRI measurement and then calculating the mean ICP curve over this time interval.
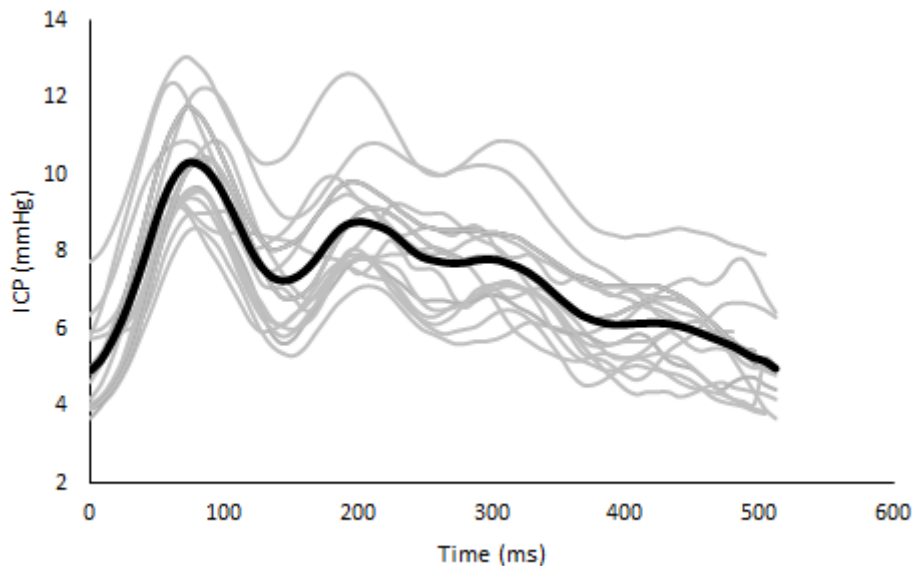
Figure 12. A composite ICP curve
All ICP curves measured over one respiratory cycle in grey and the calculated mean ICP curve in black.

In paper III the mean ICP value was calculated and registered by the patient data monitoring system (PDMS) immediately before transfer to the MRI examination was used.

When ICP had been measured in the MRI environment the signal from the ICP transducer was transferred from the investigation room, through a radiofrequency filter at the penetration panel in the shielding enclosure into the MRI-control room. Here the signal was recorded as per above.

Phase contrast MRI

All examinations had been performed with a standardized protocol. Different VENC and through plane was used for CSF measurements compared to arterial and venous measurements. The two measurements were made in immediate succession.

The examinations were analysed by one examiner blinded to the ICP curves using the freely available software SEGMENT v2.0 R5432[77].

Regions of interest were outlined manually around the internal carotid arteries, the vertebral arteries, the internal jugular veins and the spinal canal. Data was then extracted, and the flow curves transferred to Excel, where all calculations were made.

Arterial measurements

Arterial blood flow values through the internal carotid and the vertebral arteries were summarized to calculate the CBF flow curve over the cardiac cycle and then integrated over time to yield the CBF over one cardiac cycle ($ccCBF_{MR}$) in ml/stroke. $ccCBF_{MR}$ was then multiplied with the heart rate to give the CBF in ml/min.

To calculate the pulsatile component the lowest flow over the cardiac cycle was multiplied with time to give the non-pulsatile component. This was then subtracted from the $ccCBF_{MR}$, producing the pulsatile component ($ccCBF_{MRpuls}$).
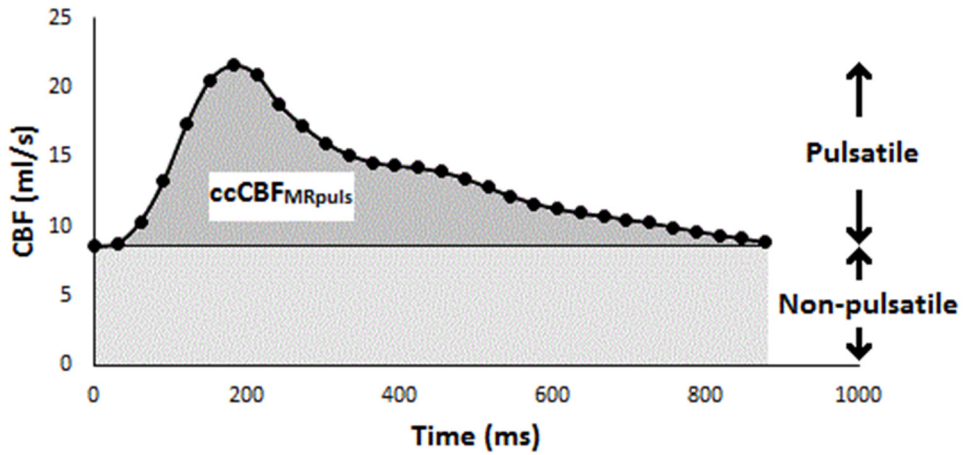
Figure 13. The cerebral blood flow over one cardiac cycle
The cerebral blood flow over one cardiac cycle, divided into the non-pulsatile component and the pulsatile component, ccCBF$_{MRpuls}$. The area under the curve represents the volume over one cardiac cycle.

Venous measurements

The flow through the internal jugular veins was summarized. In paper II and IV volume calculations required correction of this value since not all blood of venous origin flows through the IJV. This correction was done by multiplying the flow with a constant so that it equalled the measured CBF[24,60,61]

To calculate the pulsatile component of the flow (IJV$_{puls}$) the method described above for arterial measurements was used.
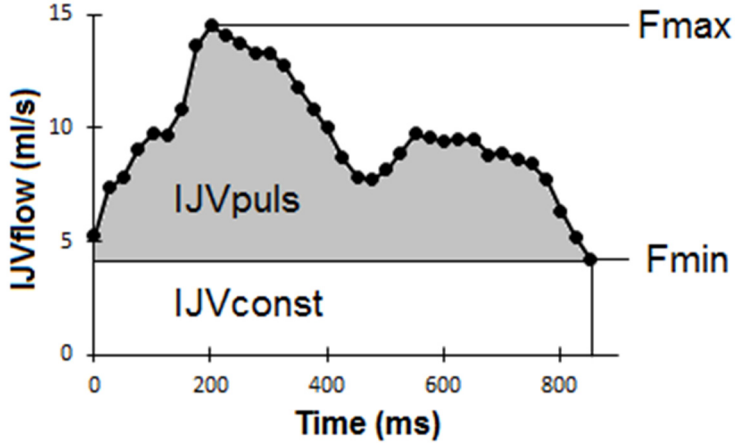
Figure 14. The venous outflow through the IJV over one cardiac cycle
The venous outflow through the internal jugular veins, IJV$_{flow}$ over one caridac cycle. The maximum flow F$_{max}$ and the minimum flow, F$_{min}$ are indicated. The grey area represents the pulsatile component, IJV$_{puls}$. The white area represents the constant component.

The venous internal jugular vein pulse ratio (IJV$_{pulsrat}$) was calculated by dividing the IJV$_{puls}$ with the total IJV flow over one cardiac cycle. The venous pulsatile index (VPI) was calculated through the formula, VPI = 100 × (F$_{max}$ − F$_{min}$)/F$_{max}$[61].

Paper I

In paper I the pulsatile component of CBF was compared to the amplitude of the ICP curve (ICP$_{amp}$), the area under the curve (AUC) of the ICP curve (AUC ICP) and the AUC of the calculated ΔICV (AUC ΔV).

ICP$_{amp}$ was calculated by subtracting the minimal ICP (ICP$_{min}$) from the maximum ICP (ICP$_{max}$) over the cardiac cycle.

The AUC ICP was calculated by integrating the ICP over the time of one cardiac cycle.

To calculate the AUC ΔV the ICP curve was transformed into a ΔICV curve. To achieve this the previously established equation

$$ICP = ICP_{eq} \times e^{E \times \Delta V},$$

was used. ICP_{eq} is defined as the steady state ICP before a change in intracranial volume, in the calculations renamed ICP_0.

The equation can be rewritten as

$$\Delta V = \frac{1}{E} \times \ln\left(\frac{\Delta ICP}{ICP_0} + 1\right)$$

Using this equation, the ICP curve can be converted to a ΔV curve.

In order to determine the elastance used in this calculation the equation can be rewritten again,

$$E = \frac{1}{\Delta V} \times \ln\left(\frac{\Delta ICP}{ICP_0} + 1\right),$$

where E is the elastance, ΔV is the aspirated volume of CSF, ICP_0 is the baseline ICP before aspiration and ΔICP is the change in ICP induced by the aspiration of CSF.

Using the registered values from the CSF aspirations and these equations, the ΔV curve could be determined and the AUC ΔV then calculated by integrating this curve over time.

The correlations were determined using linear regression.

Paper II

In this paper the ΔICV and the total flow into and out of the cranial cavity over the cardiac cycle (Flow$_{tot}$) was compared to the ICP curve.

Calculations of the change in intracranial volume over the cardiac cycle were made using the formula

$$\Delta ICV(t) = \int_{t_0}^{t} \left(CBFa(t) - CBFv(t) - CSFF(t)\right)dt,$$

where the venous blood flow had been corrected to equal the arterial inflow over the cardiac cycle as described above.

The Flow$_{tot}$ was calculated by summarizing the arterial, venous and CSF flow at each time point. All Flow$_{tot}$ values were plotted over time, thus presented as a Flow$_{tot}$ curve over the cardiac cycle (Figure 19).

The ΔICV curve was compared to the ICP curve and the Flow$_{tot}$ curve was compared to the P1 part of the ICP curve through linear regression. Student's t test was used to test the null hypothesis between paired samples.

Paper III

In this paper the VPI and the $IJV_{pulsrat}$ were calculated as per above. The values were compared to the mean ICP value registered in the PDMS immediately before the MRI examinations.

Clinical data regarding mean arterial pressure (MAP), end tidal CO_2 and temperature at the time for the MRI examination was retrieved from the PDMS.

Linear regression was used to test correlation and the Mann-Whitney U test was used to test the null hypothesis between samples.

Paper IV

To assess whether it was possible to recreate the ICP curve using the arterial cerebral inflow curve a mathematical model describing the physiology of the intracranial compartment was created. The mathematical model was constructed as an algorithm, using Matlab and then executed on a standard PC.

The mathematical model

Physics

Blood flow through distensible vessels may be described by a number of subsequent compartmental equations. The equation

$$L_k \frac{dq_k(t)}{dt} = p_k(t) - p_{k+1}(t) - R_k q_k(t)$$

describes the flow q_k from compartment k to compartment $k+1$ where L_k is the inertia (impedance) and R_k the resistance to this flow in the compartment k.
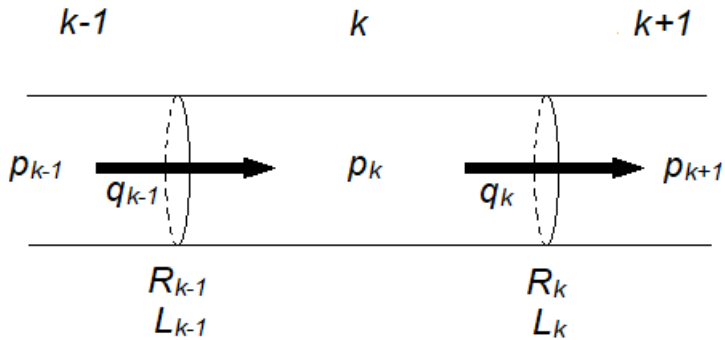
Figure 15. A compartmental model
An illustration of flow through a compartmental model. Compartments are identified as k, k-1 and k+1. Pressure (p), flow (q), resistance (R) and impedance (L) are all denoted by their compartment.

The second equation is a conservation equation. It describes the volume in compartment k as a function of the flow to and from this compartment.

$$\frac{dV_k(t)}{dt} = q_{k-1}(t) - q_k(t).$$

This equation states that the time derivate of volume in compartment k equals the difference of the time dependent flow into and out from compartment k.

The third equation relates the transmural pressure of the compartment to the stressed volume of the compartment. Transmural pressure is here defined as p_k - $p_{outside}$. The stressed volume (ΔV_k) is the volume in the compartment that is the consequence of a pressure within the compartment higher than that of the surrounding pressure, $\Delta V_k = V_k - V_{k\ unstressed}$. The importance of calculating the stressed volume lies in the fact that it is this volume that interacts with the surroundings regarding pressure.
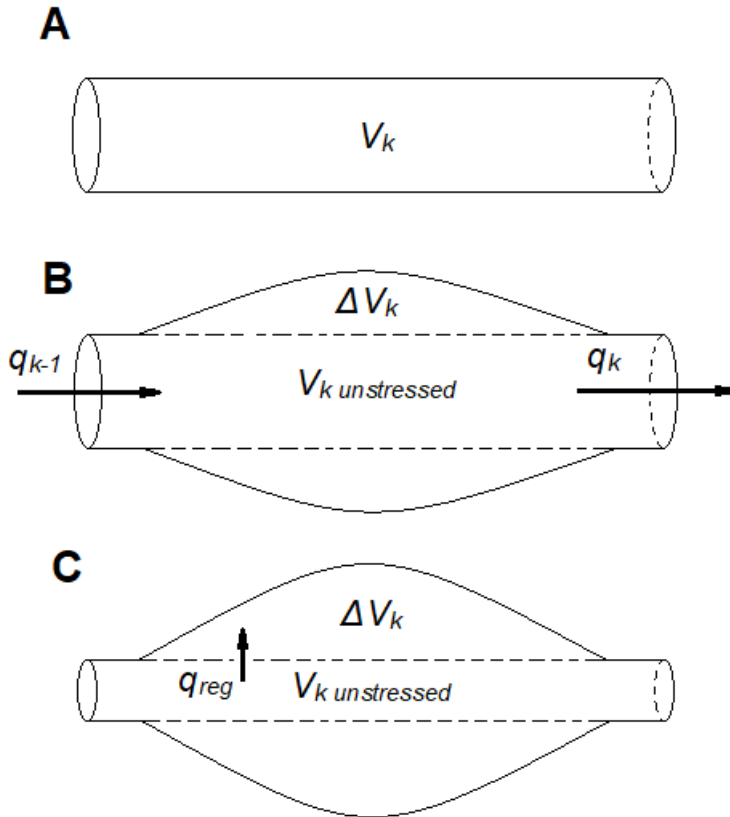
Figure 16. Illustration of stressed volume
In A a vessel is unstressed, the volume in that compartment is V_k and the internal pressure p_k equals the external pressure, $p_{outside}$. In B a larger inflow q_{k-1} than outflow q_k causes a volume expansion and a pressure increase in the vessel, which expands the stressed volume (ΔV_k) due to the increased transmural pressure, $p_k - p_{outside}$. V_k now equals $\Delta V_k + V_{k\ unstressed}$. C illustrates the effect of an additional local regulation, which simultaneously adjust the arterial compliance c_k and changes the ratio of ΔV_k and $\Delta V_{k\ unstressed}$. This redistribution of fluid is described by a flow q_{reg} between the unstressed and the stressed volumes. We emphasize that the flow q_{reg} also dependents on the compliance of the specific compartment, which is the inverse elastance of the vessel, $e_k = 1/c_k$.

The relationship is usually described by the equation

$$\Delta V_k = c_k(p_k(t) - p_{outside}),$$

where compliance of the compartment (C_k) is introduced, but frequently the non-linear relation

$$\Delta V_k = \log\big(c_k(p_k(t) - p_{outside})\big),$$

is used.

Compliance hence describes the relationship between volume and pressure within the compartment. The inverse compliance of the compartment is termed the elastance (e_k), whereas the inverse resistance of the compartment is conductivity (ρ_k). In general, all these parameters depend on material properties, universal constants and radii, thus volume of the tube element considered. In case of Poiseuille flow such relations may be derived analytically ($L_k \sim V_k^{-1}$, $R_k \sim V_k^{-2}$ and $c_k \sim V_k^{2/3}$) but in general this is not possible[97].

The model

A model simulating the intracranial hydrodynamics was created using four compartments, the arterial compartment, the venous compartment, the CSF compartment and the spinal compartment.
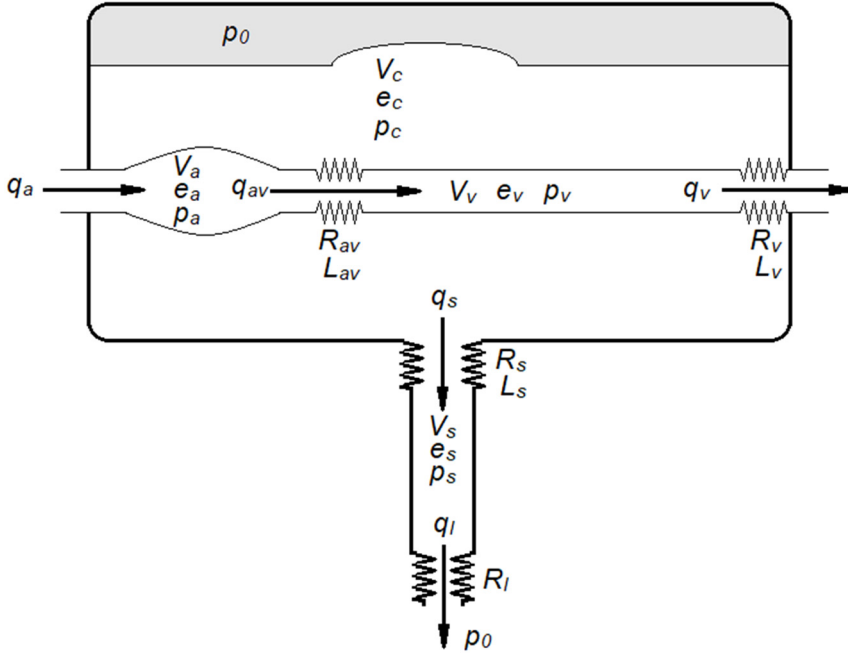
Figure 17. A drawing of the model
The different compartments illustrated in a drawing. Flow (q), volume (v), elastance (e), pressure (p), resistance (R) and impedance (L) are all denoted by the respective compartment or flow direction. P_0 equals the pressure in the brain tissue and outside the spinal cord compartment. Note that the actual flow q_s is bidirectional (as all flow may be) and the direction depends on the state of the model. However the arrows indicate the convention of positive flow for calculating purposes.

Applying the general equations above on the proposed model we arrive at a system of eight specific differential equations, which on closed form read,

$$\Delta V_a' = q_a - q_{av} + q_{reg}, \qquad\qquad [I]$$

$$\Delta V_v' = q_{av} - q_v, \qquad\qquad [II]$$

$$\Delta V_c' = q_a - q_v - q_s, \qquad\qquad [III]$$

$$\Delta V_s' = q_s - q_l, \qquad\qquad [IV]$$

$$L_s q_s' = e_c \Delta V_c - e_s \Delta V_s - R_s q_s, \qquad\qquad [V]$$

45

$$L_v q_v' = e_v \Delta V_v + e_c \Delta V_c - R_v q_v, \qquad\qquad \text{[VI]}$$

$$q_{am}' = q_{reg}, \qquad\qquad \text{[VII]}$$

$$V_{a0}' = -q_{reg}, \qquad\qquad \text{[VIII]}$$

where

$$q_{av} = \rho_{av}(e_a \Delta V_a - e_v \Delta V_v), \qquad\qquad \text{[IX]}$$

$$q_l = \rho_l e_s \Delta V_s, \qquad\qquad \text{[X]}$$

and

$$q_{reg} = \frac{q_a - q_{am}}{\tau_{reg}}. \qquad\qquad \text{[XI]}$$

Equations I-IV describe the stressed volume changes over time in the four compartments, arterial (*a*), venous (*v*), CSF (*c*) and spinal (*s*), depending on the flow between these compartments.

q_{reg}, as introduced in equation I, is the flow from unstressed to stressed volume within the arterial compartment. It is calculated through equation XI, further described below. In equation IV the model includes a possible leak from the spinal canal out from the model. This leak is however insignificant on the time scale of one heartbeat.

In equation V impedance is introduced to the flow of CSF over the foramen magnum. The flow is driven by the pressure difference between the CSF compartment and the spinal compartment and opposed by the resistance to this flow. Both may depend on the direction of flow (see below).

Equation VI introduces impedance to the flow from the venous compartment out from the model, i.e. to the systemic venous circulation. This flow is dependent on the pressure in the venous compartment, which indirectly includes the pressure put on this compartment by the pressure in the CSF compartment and the resistance to this flow.

Equation VII defines the mean arterial flow q_{am} as a weighted mean over time using an exponential weight kernel function with time constant τ_{reg}. Equivalently, the derivative of q_{am} becomes q_{reg} defined in XI. Thus, q_{reg} dependents on previous flow, providing the model with a function to adapt to rapid changes in flow through myogenic response. The concept is further developed below.

Equation VIII stipulates that the derivative of the unstressed volume, i.e. the change in unstressed volume (V_{a0}') dependents on the flow from the unstressed to the stressed volume within the arterial compartment. This equation conserves the arterial fluid in each time step of the integration when solving the equations numerically.

Equation IX describes the flow from the arterial to the venous compartment as dependent on the conductance of this flow and the difference in pressure between the two compartments.

Equation X, in the same way, defines the leak from the spinal compartment out from the model as dependent on the conductance of this flow and the pressure in the spinal compartment.

Equation XI defines q_{reg} as dependent on the weighted mean arterial flow and the current arterial flow. The mean arterial flow is weighted with a decaying history, the latter having a time constant τ_{reg}. Combining this equation with equation I implies a myogenic control, where the stressed volume is dependent on the arterial compartment's muscular contraction, which is dependent on previous inflow.

We emphasize that the parameters are not all treated as being constant and in fact we will allow some of these to depend on the state variables (the stressed volumes), since these are known to vary with vessel radii[97].

Pressures

Equations XII to XV state that stressed volumes and transmural pressures are proportional, with proportionality constant given by the vessel elastances in analogy with Ohm's law. However, later on these elastance constants are allowed to vary with the unstressed volumes[97]. After the previous equations are solved the pressure in each compartment may be calculated through these.

$$p_a = e_a \Delta V_a + p_c \qquad\qquad\qquad \text{[XII]}$$

$$p_v = e_v \Delta V_v + p_c \qquad\qquad\qquad \text{[XIII]}$$

$$p_c = e_c \Delta V_c + p_0 \qquad\qquad\qquad \text{[XIV]}$$

$$p_s = e_s \Delta V_s + p_0 \qquad\qquad\qquad \text{[XV]}$$

Varying parameters

As stated above, some of the parameters in the flow and volume equations will depend on the state of the model. The varying parameters are calculated through equations XVI to XXIII.

$$q_{reg} = \frac{(q_a - q_{am})}{\tau_{reg}}, \qquad\qquad \text{for } V_{a0} > 0, \qquad\qquad \text{[XVI]}$$

$$q_{reg} = 0, \qquad\qquad \text{otherwise,}$$

$$e_a = e_{a0} \left(\frac{n_{ea}}{\Delta V_a}\right)^{m_{ea}} \exp(-k_{ea}\, q_{reg}), \qquad\qquad \text{[XVII]}$$

$$R_{av} = R_{av0} \left(\frac{n_{R_{av}}}{V_{a0} + \Delta V_a}\right)^{m_{R_{av}}}, \qquad\qquad \text{[XVIII]}$$

$$R_v = R_{v0} / \Delta V_v^{m_{R_v}}, \qquad\qquad \text{[XIX]}$$

$$e_v = -\frac{e_{v1}(\Delta V_v)^{m_{ev1}}}{V_{v0} + \Delta V_v}, \qquad\qquad \text{for } \Delta V_v < 0, \qquad\qquad \text{[XX]}$$

$$e_v = e_{v2}(\Delta V_v)^{m_{ev2}}, \qquad\qquad \text{for } \Delta V_v \geq 0,$$

$$e_c = e_{c0} \exp(k_{ec}\, \Delta V_c), \qquad\qquad \text{[XXI]}$$

$$R_s = R_{cs}\left(1 + a_{R_s}\right), \qquad\qquad \text{for } q_s > 0, \qquad\qquad \text{[XXII]}$$

$$R_s = R_{cs}\left(1 - a_{R_s}\right), \qquad\qquad \text{for } q_s \leq 0,$$

$$L_s = L_{cs}\left(1 - b_{L_s}\right), \qquad\qquad \text{for } q_s > 0, \qquad\qquad \text{[XXIII]}$$

$$L_s = L_{cs}\left(1 + b_{L_s}\right), \qquad\qquad \text{for } q_s \leq 0.$$

In equation XVI we state that q_{reg} should be calculated according to equation XI as long as the unstressed volume in the arterial compartment is positive. By setting this condition, we define the flow to the stressed volume as dependent on q_{reg} only if there is any fluid to flow.

Equation XVII states that the elastance of the arterial compartment is dependent on the elastance in the unstressed state (e_{a0}) and the power of the stressed volume and the elastance due to muscular resistance to distension in the arterial wall (m_{ea}). It is

also exponentially related to the q_{reg} and decaying described by a negative coefficient (k_{ea}). In sum, this equation tells us that the elastance at any given moment is dependent on the stressed volume and the flow from unstressed to stressed volume at that moment.

In equation XVIII we state that the resistance to flow from the arterial to the venous compartment varies depending on a constant (k_{va}), total volume in the arterial compartment and a myogenic resistance factor (m_{Rav}). The result is that an increase in arterial radius due to increased arterial pressure will decrease resistance in the compartment. This follows Poiseuille's law.

Equation XIX states the same regarding resistance to venous outflow from the model. Resistance is dependent on the stressed volume within the compartment and a resistance factor (m_{Rv}).

Equation XX determines the elastance in the venous compartment. The veins are thin walled, with low transmural pressures and are susceptible to the intracranial pressure. Therefore, these equations follow a nonlinear relationship, based on empirical knowledge of this pressure-volume relation, which is related to the theory of flow in collapsible tubes[97-102]. The vessels change shape depending on the degree of collapse This affects resistance to flow and thereby flow through the vessels. The pressure-flow relation follows different curves, depending on whether it is collapsed or dilated. Since the change in venous flow is dependent on venous elastance (Equation VI) this effect is modelled by making elastance dependent on the degree of venous collapse or dilation, respectively.
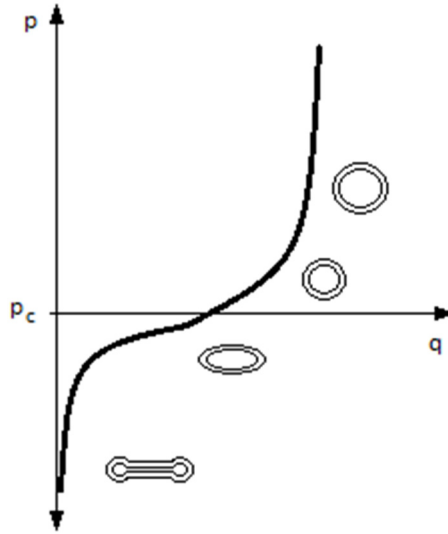
Figure 18. The typical venous pressure-flow relation
Flow (q) through a vein as a function of venous pressure (p). At high pressures the vein is distended and circular. At the pressure P_c the vein starts to collapse, becoming increasingly oval in shape, untill almost totally compressed. After Rideout, 1991.

The curve is modelled using two different equations, depending on the venous stressed volume. A set of constants then determine the slope of the two curves (e_{v1}, e_{v2}, m_{ev1} and m_{ev2}) as illustrated in Fig 18.

Equation XXI calculates the elastance of the CSF compartment depending on the elastance coefficient and the stressed volume within the CSF compartment, using an exponential elastance function in the stressed volume ΔV_c.

Equations XXII and XXIII concern the resistance and the impedance to the flow from the CSF compartment to the spinal compartment. By making them dependent on the direction of flow (the sign of q_s) it is possible to set different resistance and impedance depending on the direction of the flow.

Table 1. Parameters of the mathematical model
All parameters that are used to change the properties of the mathematical model.

Parameter	Explanation
e_{a0}	Elastance arterial compartment
R_{av0}	Resistance to flow from arterial to venous compartment
R_{v0}	Resistance to outflow from the venous compartment
e_{c0}	Elastance CSF compartment
e_s	Elastance spinal compartment
L_{cs}	Average impedance to flow from CSF to spinal compartment
R_{cs}	Average resistance to flow from CSF to spinal compartment
ρ_l	Conductance of leak flow from spinal compartment
p_0	Pressure outside of the model
b_{L_s}	Asymmetry L_{cs}-factor describing the L_{cs} impedance dependence on flow direction
a_{R_s}	Asymmetry Rcs-factor describing the Rcs resistance dependence on flow direction
L_v	Impedance to venous outflow from the model
τ_{reg}	Time constant describing the weights in the weighted average flow q_{am}
k_{ea}	Constant describing how the elastance artery depends on q_{reg}
n_{e_a}	ΔV_a normalizing constant in describing how artery elastance depends on ΔV_a
m_{ea}	Power describing how artery elastance depends on ΔV_a
$n_{R_{av}}$	ΔV_a normalizing constant in describing how artery resistance depends on ΔV_a
$m_{R_{av}}$	Power describing how artery resistance depends on ΔV_a
e_{v1}	Coefficient 1 of venous elastance describing compression
e_{v2}	Coefficient 2 of venous elastance describing dilatation
$m_{e_{v1}}$	Power describing how e_v depends on ΔV_v during compressions
$m_{e_{v2}}$	Power describing how e_v depends on ΔV_v during dilations
m_{R_v}	Power describing how venous outflow resistance depends on ΔV_v
k_{ec}	Coefficient of elastance CSF, describing how e_c depends on ΔV_c

Model derived ICP curves

For each individual the measured arterial inflow was used as q_a. With baseline settings the model was then repeated until a steady state was achieved, which took up to 120 cycles. The resulting curve was then analysed, and the parameters of the model were adjusted and run again. This process was repeated until an ICP curve as similar as possible to the individual's ICP curve was achieved.

At this point the output variables, venous outflow from the model (q_v) and CSF flow over the foramen magnum (q_s) were extracted from the model and plotted against the measured values in each individual.

Results

All values are presented as Mean ± standard deviation unless stated otherwise.

Pulsatile CBF and the ICP curve (Paper I)

Twenty-four individuals eligible for inclusion in this study were identified in the database. Eleven individuals were excluded due to suboptimal examinations. In 8 patients no reliable ICP curve had been registered in adjunct to the MRI and in 3 patients the MRI examinations were not at an appropriate level to measure CBF.

The mean age of the included patients was 50 ± 15 years, with a range from 22 to 75 years. Five patients were female.

Intracranial elastance measured and calculated through aspiration of CSF was 0.08 ± 0.03 ml/mmHg. The ICP_{amp} was 7.2 ± 3.4 mmHg. The AUC ICP was 2.01 ± 1.15 mmHg s, and the AUC ΔV was 1.18 ± 0.43 ml s.

$ccCBF_{MRpuls}$ was 4.35 ± 1.36 ml.

Individual patient data are presented in Table 2.

Table 2
Individual patient data

Age – Sex	Diagnosis	ICP$_{mean}$ (mmHg)	ccCBF$_{MRpuls}$ (ml)	ICP$_{amp}$ (mmHg)	AUC ICP (mmHg s)	AUC ΔV (ml s)
66 y – F	ICH	1.9	4.11	15.4	3.50	1.58
56 y - F	SAH	6.4	3.87	4.9	0.83	1.23
55 y - F	SAH	6.2	4.11	5.8	1.17	0.64
22 y - M	TBI	14.7	4.76	8.4	2.39	1.44
44 y - M	HC	-5.2	1.69	2.5	0.65	0.59
76 y - F	CH	1.8	3.58	4.1	1.38	0.69
34 y - M	TBI	11.7	5.52	7.1	1.77	1.44
28 y – M	TBI	11.1	7.18	8.1	2.71	1.74
38 y - M	SAH	12.7	5.82	11.8	4.66	1.76
54 y – M	TBI	3.1	3.71	4.2	0.99	1.04
64 y – M	SAH	9.0	5.04	8.6	2.51	1.54
52 y – M	CH	8.4	4.66	7.8	2.69	1.07
63 y - F	SAH	11.5	2.47	5.0	0.89	0.52

Adapted from Paper I. Age in years. F female or M male, ICH intracerebral haemorrhage, SAH subarachnoid haemorrhage, TBI traumatic brain injury, HC hydrocephalus, CH cerebellar hemorrhage, ICP$_{mean}$ mean intracranial pressure, ccCBF$_{MRpuls}$ the pulsatile component of the MRI measured CBF over one cardiac cycle, ICP$_{amp}$, ICP pulse amplitude, AUC ICP area under the pulsatile component of the ICP curve, AUC ΔV area under the pulsatile change in volume.

The correlation between ccCBF$_{MRpuls}$ and ICP$_{amp}$ was not significant (P=0.067). Both AUC ICP and AUC ΔV correlated significantly to ccCBF$_{MRpuls}$ (P=0.013 and P<0.001 respectively). Linear regression models are presented in Table 3 and linear regression plots are presented in Figure 18.

Table 3
Linear regression models of the pulsatile component of the MRI meassured CBF (ccCBFMRpuls) vs ICP pulse amplitude (ICP$_{amp}$), area under the curve of the pulsatile ICP (AUC ICP) and the area under the pulsatile change in volume (AUC ΔV)

ccCBF$_{MRpuls}$ (n = 13)	R^2	Coefficient	95% CI	Adjusted R^2	*P* value
ICP$_{amp}$	0.27	1.28	-0.10-2.67	0.21	0.067
AUC ICP	0.44	0.56	0.14-0.98	0.39	0.013
AUC ΔV	0.69	0.26	0.15-0.38	0.66	<0.001

Adapted from Paper I. R^2 coefficient of determination, 95% CI 95% confidence interval of the coefficient.
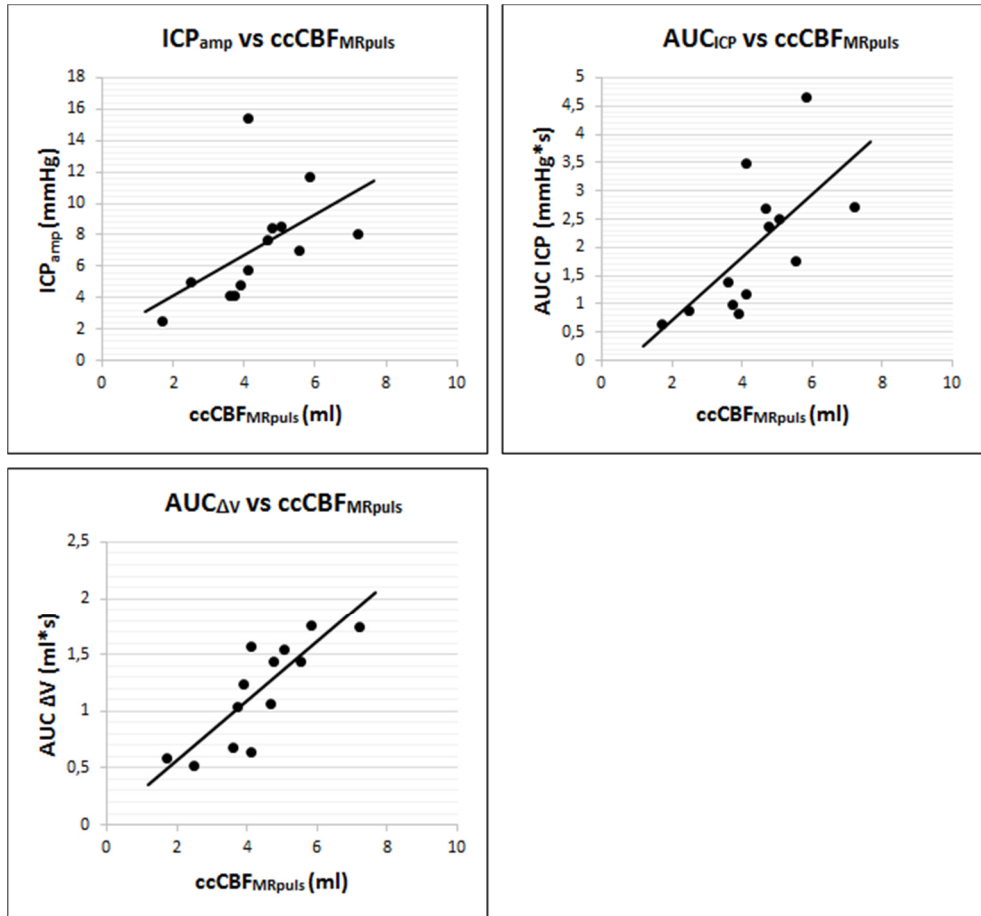
Figure 19. Regression plots
Linear regression plots of the pulsatile component of CBF over one cardiac cycle (ccCBF$_{MRpuls}$) vs the ICP amplitude (ICP$_{amp}$), the area under the curve of the pulsatile component of ICP over one cardiac cycle (AUC ICP) and the pulsatile change in volume over one cardiac cycle (AUC ΔV).

Intracranial flow-volume changes and ICP (Paper II)

A total of 10 individuals could be included. Mean age of the patients was 49 ±11 years and 9 were males. Mean ICP was 16 ±10 mmHg. ΔICV$_{max}$ was 0.68 ±0.33 ml. The calculated total flow varied over the cardiac cycle, with typically two or more peaks.
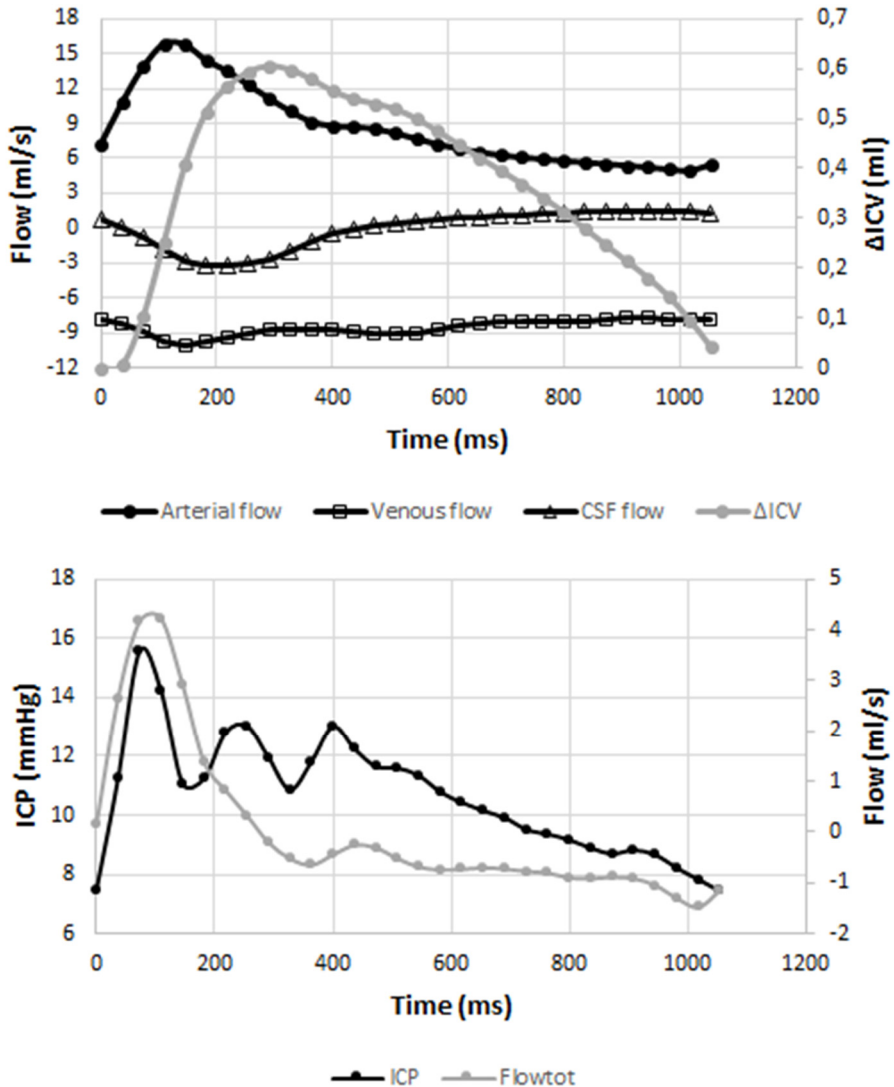
Figure 20. Flow, volume and ICP curves
The upper graph displays arterial flow, venous flow, CSF flow and the calculated change in ICV (ΔICV) over the cardiac cycle. The lower graph displays the total flow (Flow_tot) and the ICP curve. All data are from the same individual and plotted against the same timeline in the two graphs. Note the correlation between Flow_tot and ICP during the initial ICP peak (P1).

There was a correlation between ICP and ΔICV using linear regression, with a mean $R^2 = 0.41 \pm 0.14$. Using a logarithmic regression line, the correlation was strengthened, mean $R^2 = 0.47 \pm 0.13$.

The correlation between ICP and ΔICV was stronger using a logarithmic expression compared to a linear expression ($P = 0.005$).
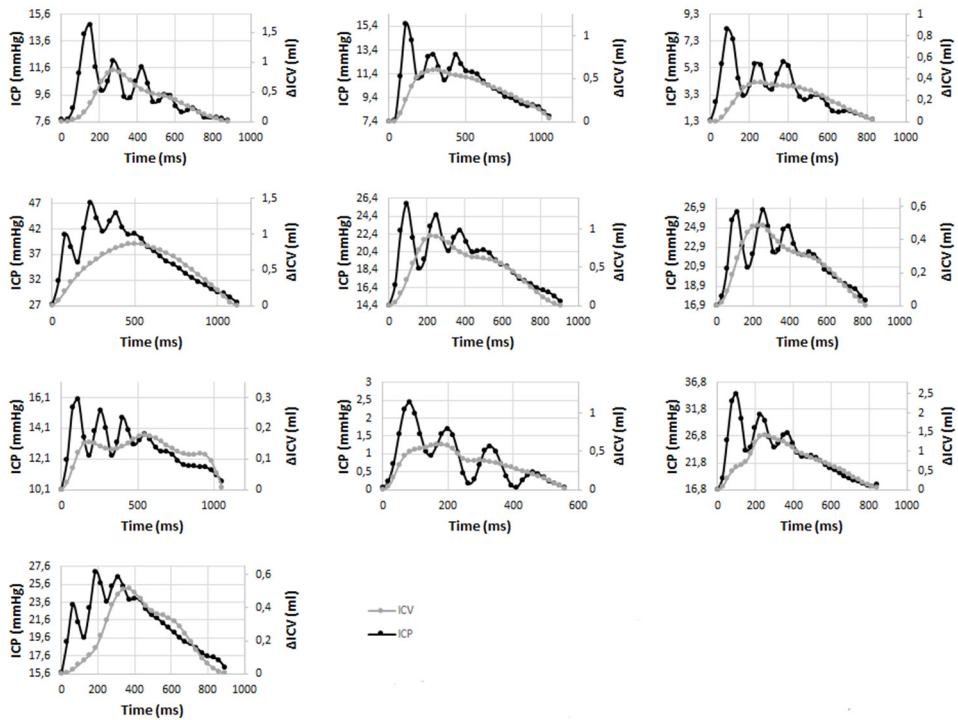
Figure 21. Volume and ICP curves
Plots of ΔICV curve and ICP curve in all individuals included in paper II.

In figure 22 the ICP is plotted against ΔICV in one individual. The values representing P1 are clearly identified as outliers. In all examinations, but one, the correlation between ICP and ΔICV was further strengthened when P1 was excluded. Using a logarithmic regression line and excluding P1 resulted in a mean $R^2 = 0.75$ ±0.15.
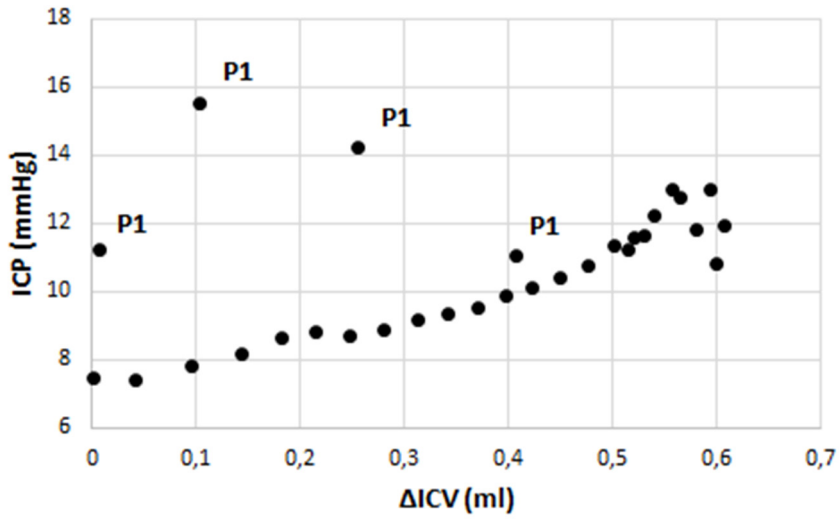
Figure 22. ICP and ΔICV plotted in one individual
Intracranial pressure (ICP) plotted against the calculated change in ICV (ΔICV) over one cardiac cycle in one individual. The points corresponding to the initial peak (P1) are apparent as outliers and marked "P1".

The ICP values representing P1 correlated to Flow$_{tot}$, mean R^2 0.88 ($\pm$0.10).

Pulsatility of venous outflow and ICP (Paper III)

Thirty-seven individuals could be included in this study. Details regarding diagnosis groups, age, sex and measurements are given in table 4.

Table 4. Diagnosis groups
Clinical data in all individuals and divided into diagnosis groups

|	TBI	SAH	Meningitis	Other	All individuals
n	15	11	5	6	37
Age (years)	44 ±14	57 ±8	52 ±10	54 ±16	50 ±14
Sex (M/F)	14 M/1 F	4 M/7 F	3 M/2 F	3 M/3F	24 M/13 F
ICPmean (mmHg)	8 ±9	9 ±7	11 ±11	10 ±7	9 ±7
MAP (mmHg)	84 ±11	94 ±14	90 ±14	92 ±6	89 ±13
CPP (mmHg)	75 ±12	85 ±15	79 ±17	82 ±11	80 ±14
CBF (ml/min)	980 ±300	990 ±220	1040 ±270	1010 ±420	1000 ±300
VPI	52 ±16	59 ±13	58 ±19	52 ±10	55 ±15
IJV$_{pulsrat}$	0.37 ±0.15	0.43 ±0.11	0.46 ±0.22	0.36 ±0.09	0.40 ±0.15

Traumatic brain injury (TBI), subarachnoid haemorrhage (SAH), meningitis and other. "Other" includes 1 multiple cerebral arterial emboli, 2 intracerebral haemorrhage, 3 hydrocephalus, and 1 meningioma. Clinical data include mean intracranial pressure (ICPmean), mean arterial pressure (MAP), cerebral perfusion pressure (CPP), cerebral blood flow (CBF), venous pulsatile index (VPI) and the pulsatile compared to total intra jugular flow ratio (IJV$_{pulsrat}$).

There was a significant difference in age between the TBI and SAH group ($p = 0.01$). There was no significant difference between the two major diagnosis groups regarding ICP, CPP and CBF.

The amount of CBF flowing through the IJV is shown in figure 22.
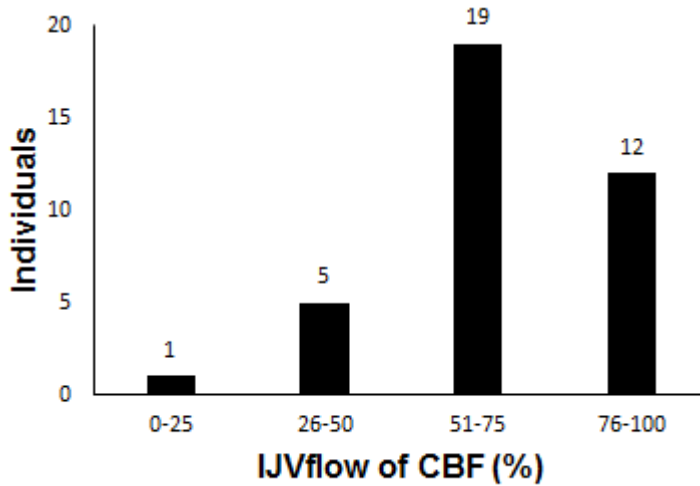
Figure 23. The distribution of venous outflow
The percentage of CBF flowing through the internal jugular veins (IJVflow of CBF) divided into 4 groups.

The $IJV_{pulsrat}$ was 0.40 ±0.15 and the VPI was 55 ±15. The amount of CBF flowing through the IJV didn´t affect these results significantly.

The $IJV_{pulsrat}$ and the VPI correlated negatively to an increase in ICP. Regression plots are presented in figure 24.
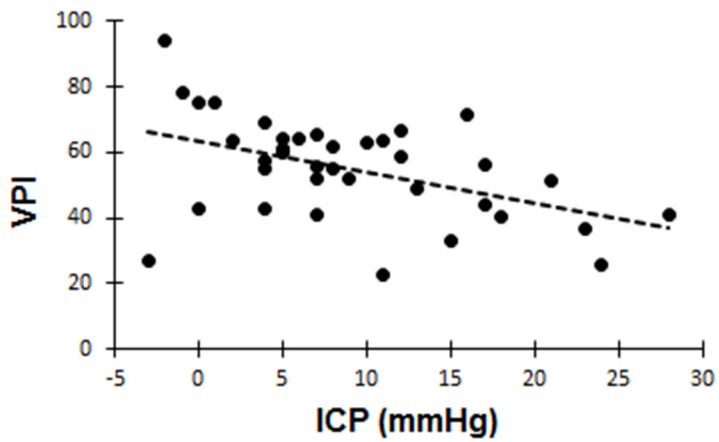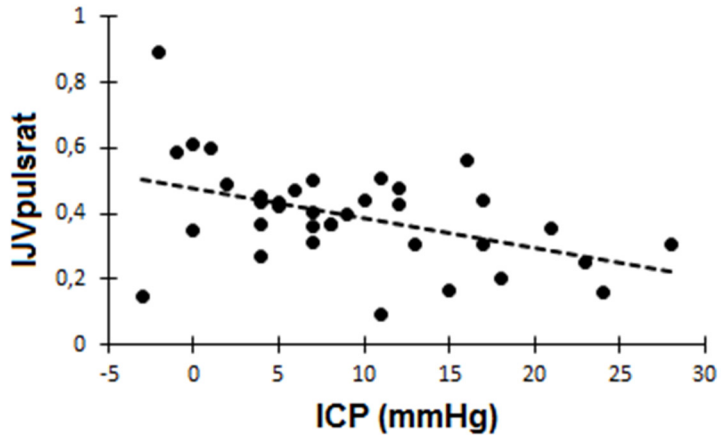
Figure 24. Regression plots of pulsatility against ICP
Regression plots of IJVpulsrat and VPI against ICP. IJVpulsrat R 0.45 (p = 0.005), VPI R 0.47 (p = 0.003).

IJV$_{pulsrat}$ and VPI had a high degree of correlation as can be observed in figure 25.
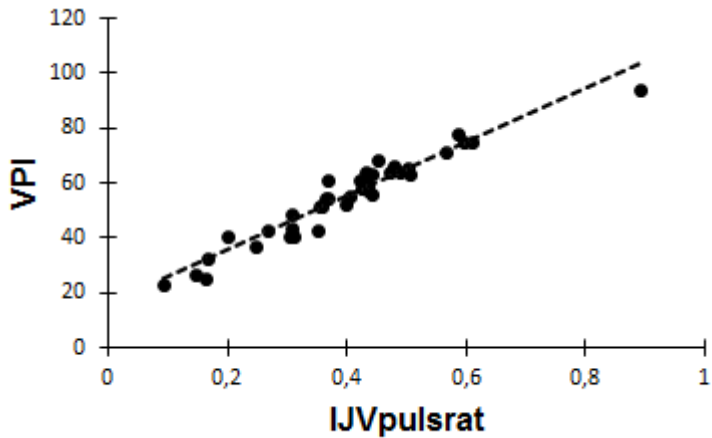
Figure 25. Regression plot of IJV$_{pulsrat}$ vs VPI
Regression plot between VPI and IJV$_{pulsrat}$. R = 0.96 (p <0.001).

Mathematical modelling (Paper IV)

Ten examinations, the same as in paper II, were found eligible for inclusion. Mean ICP value was 16 ±10 mmHg and CBF was 650 ±200 ml/min. Main diagnosis was TBI in 6 patients, subarachnoid haemorrhage in 2 patients, meningitis in 1 and obstructive hydrocephalus due to a tumour in 1.

Using the mathematical model, it was possible to achieve the multiple peak appearance of the ICP curve in all patients. A comparison between measured ICP curves and the calculated ICP curves are presented in figure 25.

In one individual (J) it wasn´t possible to fit the amplitude of the ICP curve.
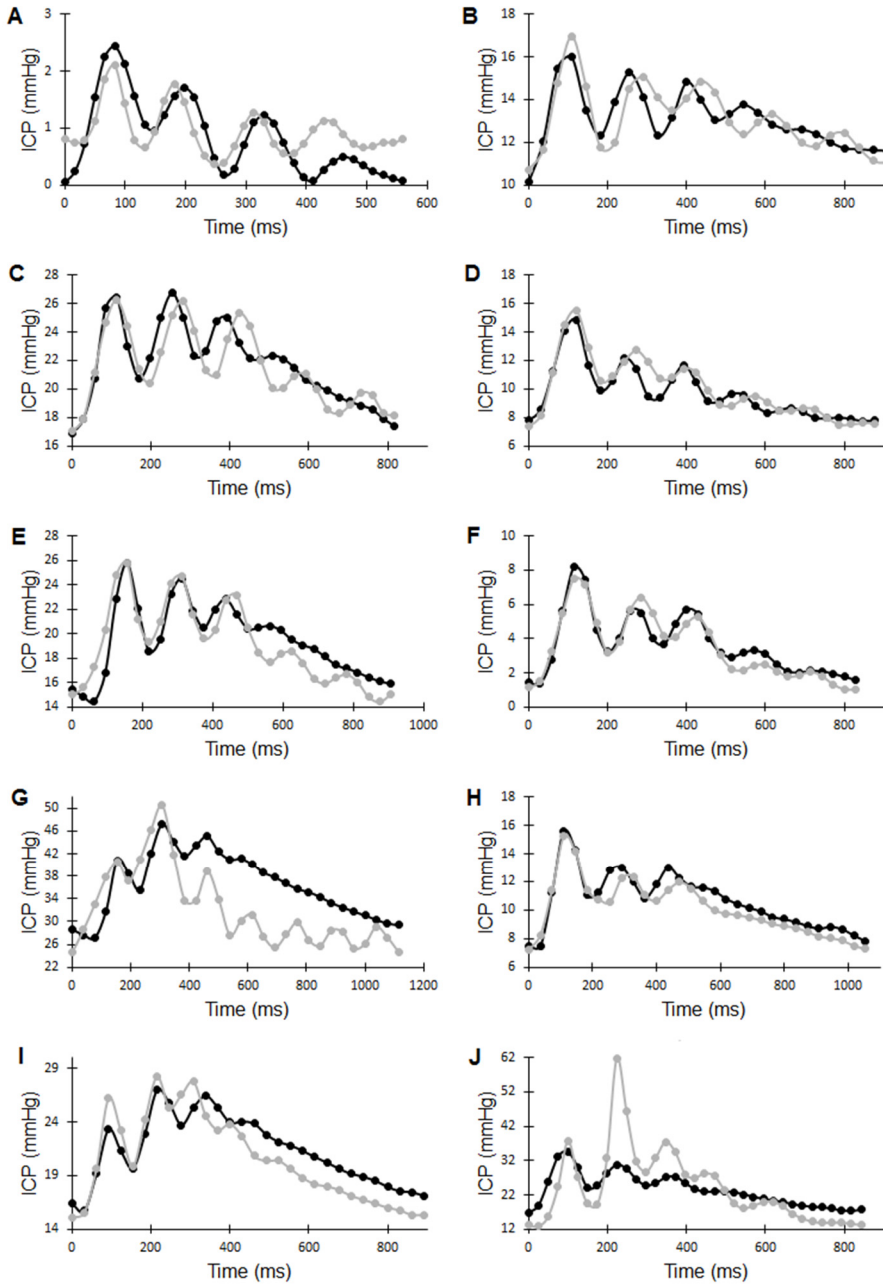
Figure 26. Measured ICP curves and model calculated ICP curves
Comparison between measured ICP curves (Black) and ICP curves calculated through the mathematical model (Grey). A good fit is achieved in all individuals except J, which has a divergent arterial inflow pattern.

64

Output data from the model compared to measured data regarding venous outflow
and CSF flow over foramen magnum are shown in figure 27.
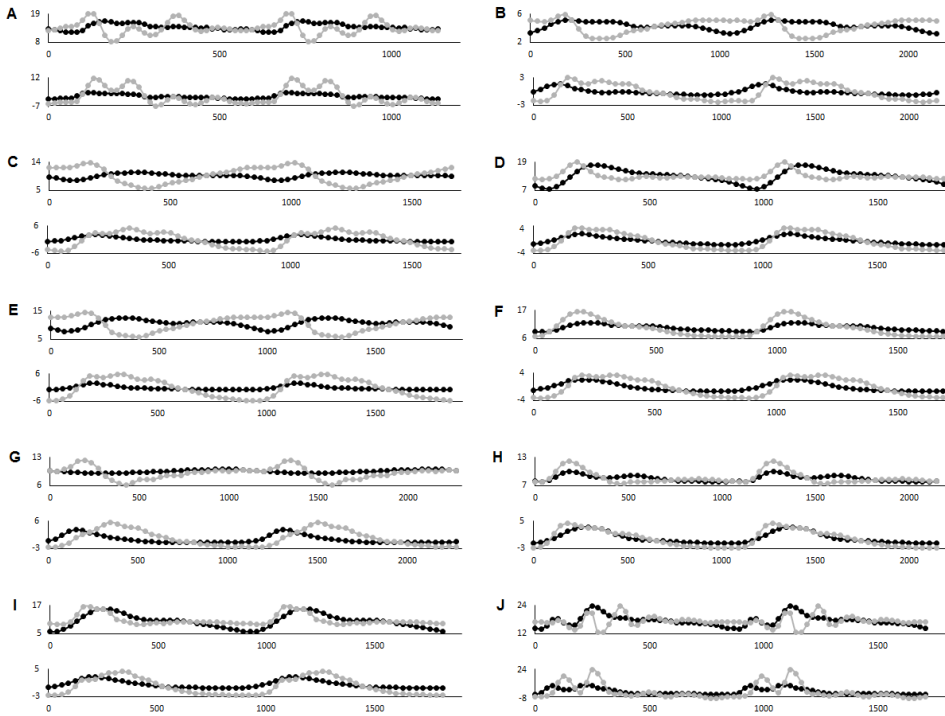
Figure 27. Output data from the mathematical model in all 10 individuals
Black curves are measured data, grey curves represents the output data from the mathematical model. For each
individual, venous outflow is shown in the upper graph and the CSF flow shown in the bottom graph.

Discussion

The physiological causes of the ICP curve morphology has yet to be fully comprehended[38]. Once fully understood it will open up for possibilities to extract valuable clinical information from the ICP curve. The papers in this thesis have the aim to explore the physiology behind the ICP curve morphology, especially with regards to the CBF.

Paper I

In paper I we explored the link between the pulsatile component of CBF and the ICP curve. The pulsatile inflow of arterial blood into the cranial cavity causes an increase in arterial cerebral blood volume (CBV_a). If the Monro-Kellie doctrine stands true over the cardiac cycle this increase in CBV_a must be immediately compensated by an outflow of cerebral venous blood and CSF. However, it has previously been observed that there exists a small increase in ΔICV over the cardiac cycle[24]. Since the content of the intracranial cavity is virtually incompressible[103] this suggests a third compensatory mechanism, probably displacement of intracranial content caudally[26].

A rapid increase in ICP is however observed when arterial inflow increases, which implies inertia in the compensatory mechanisms. The coupling between this cyclic increase in ICP and the arterial inflow is however dependent on compensatory mechanisms. Since it has been proposed that the venous outflow from the cranial cavity is dependent on the changes in the ICP over the cardiac cycle the hypothesis was that the increase in ICP should cause a pulsatile venous outflow correlated to the ICP curve. Though previous research using ultrasound Doppler technique had suggested that the venous outflow is almost non-pulsatile[104] this has been disproved by later studies[24,61]. Also, the measurements in the papers included in this thesis support a pulsatile venous outflow (I, II, III).

The pulsatile component of venous outflow and the outflow of CSF from the cranial cavity must equal the pulsatile component of the arterial inflow according to the Monro-Kellie doctrine[105]. Since net outflow of CSF over one cardiac cycle is negligible[25,106], this could be omitted. The CSF outflow at the beginning of the

cardiac cycle will attenuate the ICP increase and thereby the pressure on the veins. This decreases the amount of venous blood being forced out from the cranial cavity, while at the end of the cardiac cycle the regurgitation of CSF from the spinal canal must cause a reciprocal increase in venous outflow.

In a previous study a correlation between ICP_{amp} and CBVa was found. In paper I no correlation between the $ccCBF_{puls}$ and ICP_{amp} could be observed. An interesting finding in paper II was that the P1 of the ICP curve, which in most cases is the part defining ICP_{amp}, seems to correlate to the total flow in and out of the cranial cavity, i.e. not only arterial inflow but also venous and CSF outflow.

When taking the entire ICP curve into account, there was a correlation between ccCBF and the AUC ICP. This could be attributed to the fact that ccCBF is dependent both on the amplitude of the flow curve and the time of a cardiac cycle, while the ICP_{amp} does not take the duration of the ICP curve into account.

Since the ICP curve is dependent on the elastance of the intracranial cavity[19] the relationship between ccCBF and the AUC ICP was further explored through converting the ICP curve into a ΔV curve. This was done using the known logarithmic relationship between ICP and ΔICV[15-17]. The elastance calculations were based on extraction of CSF and the changes in ICP this resulted in. It is known that the observed elastance depends on the rate of volume change. Rapid changes of ΔICV cause more profound changes in ICP than slow changes do[107,108]. Although the measurements available for this study were done over several seconds, we postulated that they would accurately enough reflect elastance. Converting the ICP curve into an $AUC_{\Delta V}$ curve further strengthened the correlation.

These findings support the theory that there is a coupling between intracranial arterial inflow and venous outflow, with the change in ICP over the cardiac cycle acting as a transmitter.
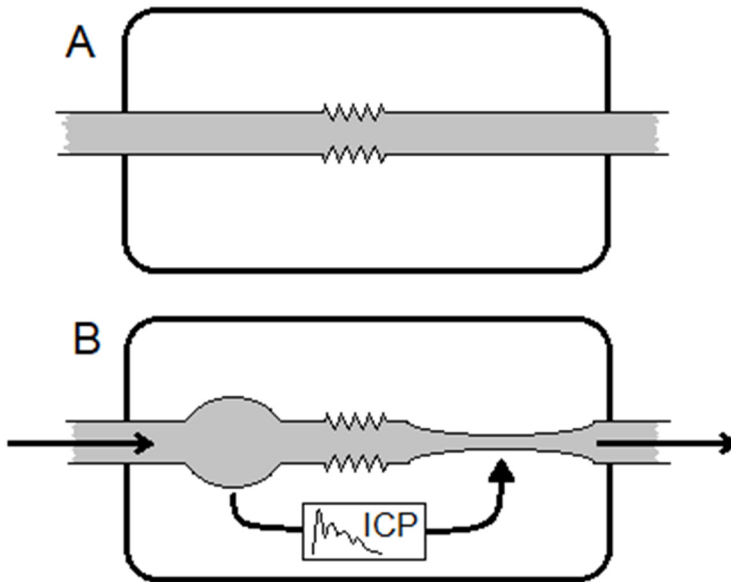
Figure 28. A simple model of the intracranial compartment
In A the intracranial compartment is depicted with an arterial compartment, followed by the resistance to the flow from arteries to veins and then a venous compartment, all in grey. In B an arterial flow into the compartment causes an expansion of the arterial compartment which causes ICP to rise. The increase in ICP causes a compression of the venous compartment with a subsequent outflow of venous blood.

The data included in this study was acquired when there was no possibility to measure ICP during the MRI examinations. This could introduce errors since there was up to 30 minutes between the MRI examinations and the ICP recordings used in the study, though the resulting errors are probably of a stochastic nature. The correlation could have been more robust if the measurements were simultaneous.

The usage of the uppermost part of the head as zero point for ICP measurements sometimes caused negative ICP values, which had to be corrected due to mathematical reasons when calculating elastance. This conversion could also introduce errors but could also minimize errors due to uncertain reference points[13].

Paper II

The purpose of the second study was to explore whether the ΔICV and intracranial flow could be correlated to the ICP curve.

It has previously been suggested that the ΔICV over the cardiac cycle could be the cause of the ICP curve[24,39,109,110] but not fully demonstrated. When comparing the ΔICV curve to the ICP curve it is obvious that the peaks of these two curves do not coincide, so that the ICP curve usually peaks before ΔICV. In paper II we demonstrated that there was a correlation of the latter part of the ICP curve when P1 was omitted. The correlation was strongest using a logarithmic regression. This is in accordance with earlier experimental studies of the ΔICV and ICP relationship[16,19-22].

This supports the theory that the ICP curve depends on the ΔICV but does not explain the peaks usually observed. A multifactorial origin of the ICP curve has previously been suggested, linking P1 to the arterial pressure wave [27] and the latter part to ΔCBV[111]. The multitude of peaks usually presented in the ICP curve are however not explained by this. To explain those a, resonance notch behaviour of the pressure wave intracranially has been suggested[32] and a mathematical model exploring these proposed features has been presented[112]. These explanations do not however take intra cranial volume changes into account and the effect of these on ICP, which has previously been demonstrated[113].

A rapid change in ICV due to sharp changes in flow into and out of the intracranial cavity could also produce a sharp initial peak. As the content of the intracranial cavity is virtually incompressible, even minute changes in ICV would lead to a rapidly increased ICP, an effect that could be dampened by other less examined factors, sometimes referred to as "brain elastance". Since the brain is incompressible[103] these factors are more likely to be of a different nature; such as the displacement of the brain caudally[26]. If these mechanisms compensate for the increasing ICV with certain inertia ICP would rise sharply and then fall rapidly as the mechanisms come into full function and the inflow decreases. This inertia could cause a resonance in the system, causing the multiple peaks usually observed.

To explore this possible feature, we compared P1 with the Flow$_{tot}$ and indeed found a strong correlation. This suggests that the increase in flow during the beginning of the cardiac cycle could be linked to the sharp increase of ICP.

The examinations in this study were performed simultaneously with the ICP registrations. We used a composite ICP curve since the MRI measurements are performed over several cardiac cycles and the respiratory cycle affects the ICP curve[114]. It must be emphasized that the time increments in this study are minute

and since there was no exact way to time correlate the ICP curve to the flow curves, small errors could exist as described in the paper.

Paper III

Paper III concerns the venous outflow and ICP. The venous outflow was early suspected to affect the ICP curve[34] and an increase in resistance to venous outflow from the cranial cavity is known to increase ICP[67-69].

If the pulsatile component of venous outflow is dependent on the ICP then the pulsatility of the venous outflow should be affected by the ICP. With increasing ICP the veins become compressed. The pressure inside the veins counteracts this compression. As the arterial inflow must be compensated by a venous outflow equal to it, the veins are kept open due to an increasing intravenous pressure as the ICP rises. This increasing pressure counteracts the compression due to increasing ICP over the cardiac cycle. An increasing amount of the venous outflow should become constant and the pulsatile component must decrease accordingly. This effect should be observed over a limited range of ICP values, since as the ICP increases the CBF becomes increasingly pulsatile[115,116] so that in extreme CPP values the venous outflow is probably affected.

The pulsatitlity of the flow through the IJV have previously been studied using VPI[61,117]. Since this method only takes maximum and minimum flow into account, we also used AUC IJV$_{pulsrat}$. which takes the entire flow curve into account. The two methods correlated well.

We observed a decrease in pulsatility with rising ICP, supporting our hypothesis. We also noted a higher pulsatility than previously reported in healthy volunteers[61,117]. This could be due to the fact that we also report a higher CBF than has been reported in healthy volunteers.

Paper IV

In paper IV we chose a different approach in order to verify our previous observational findings.

Through mathematical modelling we wanted to test the observationally supported hypothesis that it is intracranial flow and the resulting volume changes that causes the ICP changes over the cardiac cycle. Experimental studies are, using today's technology, ethically impossible to carry out. Phase contrast MRI technology has opened up for accurate measurements with high temporal resolution and ICP monitoring is a recommended procedure in the treatment of TBI[118] and commonly used in other diagnosis[119] but manipulating cerebral blood flow or other parameters influencing ICP for experimental purposes in patients cannot be done.

The usage of mathematical modelling makes it possible to perform experiments without compromising patients' safety and rights. It is however necessary to create a model that as accurately as possible mimics the physiology and expected pathophysiology.

The model constructed for this study is based on physics and known physiological properties of the intracranial cavity. Doing so we ended up with a model that closely resembles earlier proposed models[92-95]

Using this model and the measured CBF curve it was possible to construct an ICP curve similar to the ICP curve registered in the individual in all but one patient. Notably it was possible to achieve the multitude of peaks that frequently are observed on the ICP curve. Venous outflow and CSF flow over the foramen magnum calculated by the model were compared to measured values. The calculated curves were all within physiological ranges and closely resembled the measured curves in most cases. The main errors were temporal displacements of the curves.

A mathematical model is to some extent always a simplification of the reality and inherent errors in the model should be assumed. It is however interesting that this model could produce the multitude of peaks and output values so close to measured values. The model in this sense demonstrates that the ICP curve could be created by the arterial inflow into and the physiological properties of the cranial cavity.

The errors between measured values and calculated values are probably not only due to the simplifications of the model but could also be dependent on the measurements. The model calculates venous outflow at the point where venous blood leaves the cranial cavity while the exact location of this point is poorly defined. Hence, measurements of venous flow in the IJV does not necessarily represent this point. In some of the individuals more peaks can be observed on the calculated ICP curve than on the registered. This could be due to dampening of the registered ICP curve.

Synthesis

The observational evidence presented in papers I-III supports the hypothesis that the ICP curve morphology is dependent on the CBF curve and the physiological properties of the intracranial cavity.

In paper I we demonstrated the correlation between the pulsatile components of the ICP curve and the pulsatile component of CBF, while paper II links the changes in intracranial volume and the flow into and out from the cranial cavity to the ICP curve.

Paper III presents evidence that the ICP and the venous outflow pattern are associated, further linking ICP curve morphology to cerebral blood volume.

In paper IV it was shown that a mathematical model could mimic the morphology of the ICP curve, including the multitude of peaks using only arterial inflow to the cranial compartment and known physiological features.

Conclusions

There was no significant correlation between ICP_{amp} and the $ccCBF_{MRpuls}$.

There is a significant correlation between the AUC ICP and the $ccCBF_{MRpuls}$.

Using calculated elastance to modify this curve into an ΔV curve before calculating AUC improved the correlation.

The latter part of the ICP curve correlates to ΔICV.

The correlation between the ICP curve and ΔICV seems to be of an exponential nature in vivo.

P1 of the ICP curve correlates to the $Flow_{tot}$.

The pulsatility of the flow in the IJV is attenuated with increasing ICP.

The VPI and AUC method for determining pulsatility of IJV flow are interchangeable.

The mathematical model presented, using physics and known physiological properties of the intracranial cavity, could reasonably well reproduce the ICP curve, including the multitude of peaks.

Above findings support the theory that the physiological properties of the cranial cavity in conjunction with cerebral blood flow shape the ICP curve.

Future prospects

Clinical studies

The field of intracranial hydrodynamics and the ICP curve morphology has clinically relevant potential and should be further explored. This can be done by observational studies in humans and mathematical modelling.

Although this thesis adds knowledge to the area of understanding the ICP curve, further studies are required to fully explain the mechanisms behind it. The effects of CBF, venous outflow and CSF flow on the ICP curve under different conditions should be explored. If the physiology and pathophysiology is fully understood it opens up for the possibility to extract clinically useful information from the ICP curve.

Phase contrast could be used to study the intracranial fluid dynamics. At present it cannot produce complete beat to beat measurements which can be compared to the ICP curve but developments in this area are underway[75,120]. The method has until now been of mainly experimental use but the possibilities to be used in the clinical settings deserves attention.

Mathematical modelling

The mathematical model provides a promising method to explore the intracranial hydrodynamics though further development of the proposed model is required. It makes it possible to undertake theoretical studies circumventing problems arising in human studies. Though this thesis contributes with a first step in the validation of a model, this must be furthered.

Acknowledgements

Several persons have contributed greatly to my work and made this thesis possible. To thank them all would require a book in itself and I am forever grateful for their support and help. Invaluable support has been provided by:

Peter Reinstrup, my supervisor who introduced me to neuro intensive care and the field of intracranial pressure and cerebral blood flow. Always supporting and ready for intellectual discussions. A friend.

Johnny Ottesen, my co-supervisor. He introduced me to the fascinating world of mathematical modelling and brushed up my mathematical skills with friendly patience.

Erik Ryding, my co-supervisor, helping me see things from different perspectives and bringing his intellect into physiological discussions.

Karin Hesselgard. my co-supervisor. Always with good advice, constructive critique and supervising my supervisor.

Martin Ugander, who once opened the door to phase contrast MRI and its possibilities.

Eric Bloomfield and Sven Söderström, co-authors.

Carolina Samuelsson, Johan Persson and Jonas Åkesson, my superiors, providing me with precious time to complete this thesis. Invaluable support.

All my colleagues at the Anaesthesiology/Intensive care department in Malmö, who every day make me want to aim higher and try harder. A special thank you to my close colleagues and friends at the intensive care department, present and former.

The staff at the intensive care unit in Malmö, always providing a light in the darkness, always willing to move the mountain.

Colleagues and staff at the Department of Otorhinolaryngology at Skånes University Hospital. This thesis would literally have died without your expertise.

Arne Johansson and Einar Vernersson, former colleagues, sharing their wisdom and experience.

Jan Frennström, providing linguistical support of great help pro bono.

Åsa Unnerbäck, for being an excellent mother and supportive of my efforts. Also surprised me by turning out to be a linguistical expert, who's help has been invaluable.

Elias, Bea and Vilgot, my beloved children, who picks me up and sets my priorities straight. Your love carries me.

My parents, Dag och Margareta. Always supporting in thought and deed. I´m here because of you-

My sister Magdalena and her family, always there with a warm friendship.

Per and Marianne Kronqvist, always ready to help when help is needed.

References

1. Maxeiner H, Behnke M. Intracranial volume, brain volume, reserve volume and morphological signs of increased intracranial pressure--a post-mortem analysis. Legal medicine (Tokyo, Japan) 2008;10:293-300.

2. Reinstrup P, Ryding E, Ohlsson T, Dahm PL, Uski T. Cerebral blood volume (CBV) in humans during normo- and hypocapnia: influence of nitrous oxide (N(2)O). Anesthesiology 2001;95:1079-82.

3. Guyton AC, Hall JE. Textbook of medical physiology. Philadelphia: Elsevier Saunders; 2006:764-7.

4. Wright BL, Lai JT, Sinclair AJ. Cerebrospinal fluid and lumbar puncture: a practical review. Journal of neurology 2012;259:1530-45.

5. Ekstedt J. CSF hydrodynamic studies in man. 2. Normal hydrodynamic variables related to CSF pressure and flow. Journal of neurology, neurosurgery, and psychiatry 1978;41:345-53.

6. Sakka L, Coll G, Chazal J. Anatomy and physiology of cerebrospinal fluid. European annals of otorhinolaryngology, head and neck diseases 2011;128:309-16.

7. Monro A. Observations on the structure and functions of the nervous system. Illustrated with tables. By Alexander Monro. Edinburgh: printed for, and sold by, William Creech; and Joseph Johnson, London; 1783.

8. Kellie G. An Account of the Appearances Observed in the Dissection of Two of Three Individuals Presumed to Have Perished in the Storm of the 3d, and Whose Bodies Were Discovered in the Vicinity of Leith on the Morning of the 4th, November 1821; with Some Reflections on the Pathology of the Brain: Part I. Transactions Medico-Chirurgical Society of Edinburgh 1824;1:84-122.

9. Burrows G. On Disorders of the Cerebral Circulation, and on the Connection between Affections of the Brain and Diseases of the Heart. The Medico-chirurgical review 1846;4:34-48.

10. Quincke HF. Uber Meningitis serosa, von H. Quincke. Leipzig: Breitkopf und Härtel; 1893.

11. Hodgson JS. Combined ventricular and lumbar puncture in the diagnosis of brain tumor: Further studies. Journal of the American Medical Association 1928;90:1524-6.

12. Guillaume J, Janny P. [Continuous intracranial manometry; physiopathologic and clinical significance of the method]. La Presse medicale 1951;59:953-5.

13.   Lundberg N. Continuous recording and control of ventricular fluid pressure in neurosurgical practice. Acta psychiatrica Scandinavica Supplementum 1960;36:1-193.

14.   Ryder HW, Espey FF, Kimbell FD, et al. The elasticity of the cerebrospinal venous bed. The Journal of laboratory and clinical medicine 1953;42:944.

15.   Langfitt TW, Weinstein JD, Kassell NF. Cerebral vasomotor paralysis produced by intracranial hypertension. Neurology 1965;15:622-41.

16.   Lofgren J, von Essen C, Zwetnow NN. The pressure-volume curve of the cerebrospinal fluid space in dogs. Acta neurologica Scandinavica 1973;49:557-74.

17.   Miller JD, J. G. Intracranial pressure: experimental and clinical aspects. Intracranial pressure. Berlin: Springer; 1972:270-4.

18.   Lofgren J, Zwetnow NN. Cranial and spinal components of the cerebrospinal fluid pressure-volume curve. Acta neurologica Scandinavica 1973;49:575-85.

19.   Avezaat CJ, van Eijndhoven JH, Wyper DJ. Cerebrospinal fluid pulse pressure and intracranial volume-pressure relationships. Journal of neurology, neurosurgery, and psychiatry 1979;42:687-700.

20.   Marmarou A, Shulman K, LaMorgese J. Compartmental analysis of compliance and outflow resistance of the cerebrospinal fluid system. Journal of neurosurgery 1975;43:523-34.

21.   Marmarou A, Shulman K, Rosende RM. A nonlinear analysis of the cerebrospinal fluid system and intracranial pressure dynamics. Journal of neurosurgery 1978;48:332-44.

22.   Ryder HW, Espey FF, Kimbell FD, et al. The mechanism of the change in cerebrospinal fluid pressure following an induced change in the volume of the fluid space. The Journal of laboratory and clinical medicine 1953;41:428-35.

23.   Alperin N, Sivaramakrishnan A, Lichtor T. Magnetic resonance imaging-based measurements of cerebrospinal fluid and blood flow as indicators of intracranial compliance in patients with Chiari malformation. Journal of neurosurgery 2005;103:46-52.

24.   Alperin NJ, Lee SH, Loth F, Raksin PB, Lichtor T. MR-Intracranial pressure (ICP): a method to measure intracranial elastance and pressure noninvasively by means of MR imaging: baboon and human study. Radiology 2000;217:877-85.

25.   Baledent O, Henry-Feugeas MC, Idy-Peretti I. Cerebrospinal fluid dynamics and relation with blood flow: a magnetic resonance study with semiautomated cerebrospinal fluid segmentation. Investigative radiology 2001;36:368-77.

26.   Greitz D, Wirestam R, Franck A, Nordell B, Thomsen C, Stahlberg F. Pulsatile brain movement and associated hydrodynamics studied by magnetic resonance phase imaging. The Monro-Kellie doctrine revisited. Neuroradiology 1992;34:370-80.

27.   Cardoso ER, Rowan JO, Galbraith S. Analysis of the cerebrospinal fluid pulse wave in intracranial pressure. Journal of neurosurgery 1983;59:817-21.

28.   Gega A, Utsumi S, Iida Y, Iida N, Tsuneda S. Analysis of the wave pattern of CSF pulse wave. In: Shulman K, Marmarou A, Miller J, Becker D, Hochwald G, Brock M, eds. Intracranial pressure IV. Berlin: Springer; 1980:180-90.

29. Dunbar HS, Guthrie TC, Karpell B. A study of the cerebrospinal fluid pulse wave. Archives of neurology 1966;14:624-30.

30. Bering EA, Jr. Choroid plexus and arterial pulsation of cerebrospinal fluid; demonstration of the choroid plexuses as a cerebrospinal fluid pump. AMA archives of neurology and psychiatry 1955;73:165-72.

31. Takizawa K, Matsumae M, Hayashi N, et al. The choroid plexus of the lateral ventricle as the origin of CSF pulsation is questionable. Neurologia medico-chirurgica 2018;58:23-31.

32. Wagshul ME, Kelly EJ, Yu HJ, Garlick B, Zimmerman T, Egnor MR. Resonant and notch behavior in intracranial pressure dynamics. Journal of neurosurgery Pediatrics 2009;3:354-64.

33. Zou R, Park EH, Kelly EM, Egnor M, Wagshul ME, Madsen JR. Intracranial pressure waves: characterization of a pulsation absorber with notch filter properties using systems analysis: laboratory investigation. Journal of neurosurgery Pediatrics 2008;2:83-94.

34. Hamit HF, Beall AC, Jr., Debakey ME. Hemodynamic influences upon brain and cerebrospinal fluid pulsations and pressures. The Journal of trauma 1965;5:174-84.

35. Adolph RJ, Fukusumi H, Fowler NO. Origin of cerebrospinal fluid pulsations. The American journal of physiology 1967;212:840-6.

36. Avezaat CJJ, van Eijndhoven JHM, de Jong DA, Moolenaar WCJ. A new method of monitoring intracranial volume/pressure relationship. In: Beks JWF, Bosch DA, Brock M, editors. Intracranial Pressure III; 1976 1976//; Berlin, Heidelberg: Springer Berlin Heidelberg. p. 308-13.

37. Hu X, Glenn T, Scalzo F, et al. Intracranial pressure pulse morphological features improved detection of decreased cerebral blood flow. Physiological measurement 2010;31:679-95.

38. Baledent O, Czosnyka M, Czosnyka ZH. Brain pulsations enlightened. Acta neurochirurgica 2018;160:225-7.

39. Baledent O, Fin L, Khuoy L, et al. Brain hydrodynamics study by phase-contrast magnetic resonance imaging and transcranial color doppler. J Magn Reson Imaging 2006;24:995-1004.

40. Baledent O, Gondry-Jouet C, Meyer ME, et al. Relationship between cerebrospinal fluid and blood dynamics in healthy volunteers and patients with communicating hydrocephalus. Investigative radiology 2004;39:45-55.

41. Losasso TJ, Muzzi DA, Meyer FB, Sharbrough FW. Electroencephalographic monitoring of cerebral function during asystole and successful cardiopulmonary resuscitation. Anesthesia and analgesia 1992;75:1021-4.

42. Lee JM, Grabb MC, Zipfel GJ, Choi DW. Brain tissue responses to ischemia. The Journal of clinical investigation 2000;106:723-31.

43. van Mook WN, Rennenberg RJ, Schurink GW, et al. Cerebral hyperperfusion syndrome. The Lancet Neurology 2005;4:877-88.

44. Schimmel SJ, Acosta S, Lozano D. Neuroinflammation in traumatic brain injury: A chronic response to an acute injury. Brain circulation 2017;3:135-42.

45. Stocchetti N, Maas AI. Traumatic intracranial hypertension. The New England journal of medicine 2014;371:972.

46. Gopinath SP, Robertson CS, Contant CF, et al. Jugular venous desaturation and outcome after head injury. Journal of neurology, neurosurgery, and psychiatry 1994;57:717-23.

47. Nordstrom CH, Reinstrup P, Xu W, Gardenfors A, Ungerstedt U. Assessment of the lower limit for cerebral perfusion pressure in severe head injuries by bedside monitoring of regional energy metabolism. Anesthesiology 2003;98:809-14.

48. Poon WS, Ng SC, Chan MT, Lam JM, Lam WW. Cerebral blood flow (CBF)-directed management of ventilated head-injured patients. Acta neurochirurgica Supplement 2005;95:9-11.

49. Snell RS. Clinical anatomy for medical students. Boston: Little, Brown; 1995.

50. Marks MP, Pelc NJ, Ross MR, Enzmann DR. Determination of cerebral blood flow with a phase-contrast cine MR imaging technique: evaluation of normal subjects and patients with arteriovenous malformations. Radiology 1992;182:467-76.

51. Kety SS, Schmidt CF. The determination of cerebral blood flow in man by the use of nitrous oxide in low concentrations. American Journal of Physiology 1945;143:53-66.

52. Spilt A, Box FM, van der Geest RJ, et al. Reproducibility of total cerebral blood flow measurements using phase contrast magnetic resonance imaging. J Magn Reson Imaging 2002;16:1-5.

53. Lassen NA. Cerebral blood flow and oxygen consumption in man. Physiological reviews 1959;39:183-238.

54. Donnelly J, Budohoski KP, Smielewski P, Czosnyka M. Regulation of the cerebral circulation: bedside assessment and clinical implications. Critical care (London, England) 2016;20:129.

55. Jordan JD, Powers WJ. Cerebral autoregulation and acute ischemic stroke. American journal of hypertension 2012;25:946-50.

56. Sanchez-Porras R, Santos E, Czosnyka M, Zheng Z, Unterberg AW, Sakowitz OW. 'Long' pressure reactivity index (L-PRx) as a measure of autoregulation correlates with outcome in traumatic brain injury patients. Acta neurochirurgica 2012;154:1575-81.

57. Schalen W, Messeter K, Nordstrom CH. Cerebral vasoreactivity and the prediction of outcome in severe traumatic brain lesions. Acta anaesthesiologica Scandinavica 1991;35:113-22.

58. Kramer AH, Couillard PL, Zygun DA, Aries MJ, Gallagher CN. Continuous assessment of "optimal" cerebral perfusion pressure in traumatic brain injury: a cohort study of feasibility, reliability, and relation to outcome. Neurocritical care 2018.

59. Steiner LA, Czosnyka M, Piechnik SK, et al. Continuous monitoring of cerebrovascular pressure reactivity allows determination of optimal cerebral perfusion pressure in patients with traumatic brain injury. Critical care medicine 2002;30:733-8.

60. Doepp F, Schreiber SJ, von Munster T, Rademacher J, Klingebiel R, Valdueza JM. How does the blood leave the brain? A systematic ultrasound analysis of cerebral venous drainage patterns. Neuroradiology 2004;46:565-70.

61. Stoquart-Elsankari S, Lehmann P, Villette A, et al. A phase-contrast MRI study of physiologic cerebral venous flow. Journal of cerebral blood flow and metabolism : official journal of the International Society of Cerebral Blood Flow and Metabolism 2009;29:1208-15.

62. Epstein HM, Linde HW, Crampton AR, Ciric IS, Eckenhoff JE. The vertebral venous plexus as a major cerebral venous outflow tract. Anesthesiology 1970;32:332-7.

63. Dilenge D, Perey B. An angiographic study of the meningorachidian venous system. Radiology 1973;108:333-7.

64. Alperin N, Hushek SG, Lee SH, Sivaramakrishnan A, Lichtor T. MRI study of cerebral blood flow and CSF flow dynamics in an upright posture: the effect of posture on the intracranial compliance and pressure. Acta neurochirurgica Supplement 2005;95:177-81.

65. Magnaes B. Body position and cerebrospinal fluid pressure. Part 1: clinical studies on the effect of rapid postural changes. Journal of neurosurgery 1976;44:687-97.

66. Kenning JA, Toutant SM, Saunders RL. Upright patient positioning in the management of intracranial hypertension. Surgical neurology 1981;15:148-52.

67. Feldman Z, Kanter MJ, Robertson CS, et al. Effect of head elevation on intracranial pressure, cerebral perfusion pressure, and cerebral blood flow in head-injured patients. Journal of neurosurgery 1992;76:207-11.

68. Ng I, Lim J, Wong HB. Effects of head posture on cerebral hemodynamics: its influences on intracranial pressure, cerebral perfusion pressure, and cerebral oxygenation. Neurosurgery 2004;54:593-7; discussion 8.

69. Schulz-Stubner S, Thiex R. Raising the head-of-bed by 30 degrees reduces ICP and improves CPP without compromising cardiac output in euvolemic patients with traumatic brain injury and subarachnoid haemorrhage: a practice audit. European journal of anaesthesiology 2006;23:177-80.

70. Bateman GA. The pathophysiology of idiopathic normal pressure hydrocephalus: cerebral ischemia or altered venous hemodynamics? AJNR American journal of neuroradiology 2008;29:198-203.

71. Williams H. The venous hypothesis of hydrocephalus. Medical hypotheses 2008;70:743-7.

72. Myerson SG, Francis J, Neubauer S. Cardiovascular magnetic resonance. Oxford: Oxford University Press; 2010.

73. Bryant DJ, Payne JA, Firmin DN, Longmore DB. Measurement of flow with NMR imaging using a gradient pulse and phase difference technique. Journal of computer assisted tomography 1984;8:588-93.

74. Enzmann DR, Ross MR, Marks MP, Pelc NJ. Blood flow in major cerebral arteries measured by phase-contrast cine MR. AJNR American journal of neuroradiology 1994;15:123-9.

75. Spritzer CE, Pelc NJ, Lee JN, Evans AJ, Sostman HD, Riederer SJ. Rapid MR imaging of blood flow with a phase-sensitive, limited-flip-angle, gradient recalled pulse sequence: preliminary experience. Radiology 1990;176:255-62.

76. Evans AJ, Iwai F, Grist TA, et al. Magnetic resonance imaging of blood flow with a phase subtraction technique. In vitro and in vivo validation. Investigative radiology 1993;28:109-15.

77. Heiberg E, Sjögren J, Ugander M, Carlsson M, Engblom H, Arheden HJBmi. Design and validation of Segment-freely available software for cardiovascular image analysis. 2010;10:1.

78. Koerte I, Haberl C, Schmidt M, et al. Inter- and intra-rater reliability of blood and cerebrospinal fluid flow quantification by phase-contrast MRI. J Magn Reson Imaging 2013;38:655-62.

79. van der Geest RJ, Niezen RA, van der Wall EE, de Roos A, Reiber JH. Automated measurement of volume flow in the ascending aorta using MR velocity maps: evaluation of inter- and intraobserver variability in healthy volunteers. Journal of computer assisted tomography 1998;22:904-11.

80. Buonocore MH, Bogren H. Factors influencing the accuracy and precision of velocity-encoded phase imaging. Magnetic resonance in medicine 1992;26:141-54.

81. Sidhu PS. Ultrasound of the carotid and vertebral arteries. British medical bulletin 2000;56:346-66.

82. Alperin N, Lee SH, Sivaramakrishnan A, Hushek SG. Quantifying the effect of posture on intracranial physiology in humans by MRI flow studies. J Magn Reson Imaging 2005;22:591-6.

83. Zarrinkoob L, Ambarki K, Wahlin A, Birgander R, Eklund A, Malm J. Blood flow distribution in cerebral arteries. Journal of cerebral blood flow and metabolism : official journal of the International Society of Cerebral Blood Flow and Metabolism 2015;35:648-54.

84. Parent A. Carpenter's Human neuroanatomy. Baltimore: Williams & Wilkins; 1996.

85. Clarot F, Callonnec F, Douvrin F, et al. Giant cervical epidural veins after lumbar puncture in a case of intracranial hypotension. AJNR American journal of neuroradiology 2000;21:787-9.

86. Enzmann DR, Pelc NJ. Cerebrospinal fluid flow measured by phase-contrast cine MR. AJNR American journal of neuroradiology 1993;14:1301-7; discussion 9-10.

87. Wahlin A, Ambarki K, Hauksson J, Birgander R, Malm J, Eklund A. Phase contrast MRI quantification of pulsatile volumes of brain arteries, veins, and cerebrospinal fluids compartments: repeatability and physiological interactions. J Magn Reson Imaging 2012;35:1055-62.

88. Hodgkin AL, Huxley AF. A quantitative description of membrane current and its application to conduction and excitation in nerve. 1952;117:500-44.

89. Noble D. Cardiac Action and Pacemaker Potentials based on the Hodgkin-Huxley Equations. Nature 1960;188:495.

90. Gavaghan D, Garny A, Maini PK, Kohl P. Mathematical models in physiology. Philosophical transactions Series A, Mathematical, physical, and engineering sciences 2006;364:1099-106.

91. Ottesen JT, Olufsen MS, Larsen JK. Applied mathematical models in human physiology 2004.

92. Czosnyka M, Piechnik S, Richards HK, Kirkpatrick P, Smielewski P, Pickard JD. Contribution of mathematical modelling to the interpretation of bedside tests of cerebrovascular autoregulation. Journal of neurology, neurosurgery, and psychiatry 1997;63:721-31.

93. Ursino M, Lodi CA. A simple mathematical model of the interaction between intracranial pressure and cerebral hemodynamics. Journal of applied physiology (Bethesda, Md : 1985) 1997;82:1256-69.

94. Ambarki K, Baledent O, Kongolo G, Bouzerar R, Fall S, Meyer ME. A new lumped-parameter model of cerebrospinal hydrodynamics during the cardiac cycle in healthy volunteers. IEEE transactions on bio-medical engineering 2007;54:483-91.

95. Linninger AA, Tsakiris C, Zhu DC, et al. Pulsatile cerebrospinal fluid dynamics in the human brain. IEEE transactions on bio-medical engineering 2005;52:557-65.

96. Martin BA, Reymond P, Novy J, Baledent O, Stergiopulos N. A coupled hydrodynamic model of the cardiovascular and cerebrospinal fluid system. American journal of physiology Heart and circulatory physiology 2012;302:H1492-509.

97. Rideout VC. Mathematical and computer modeling of physiological systems. Englewood Cliffs, N.J.: Prentice Hall; 1991.

98. Low H, Chew YJM, Engineering B, Computing. Pressure/flow relationships in collapsible tubes: effects of upstream pressure fluctuations. 1991;29:217-21.

99. Pedley T, Luo XJT, Dynamics CF. Modelling flow and oscillations in collapsible tubes. 1998;10:277-94.

100. Pedley T, Pihler-Puzović DJS. Flow and oscillations in collapsible tubes: Physiological applications and low-dimensional models. 2015;40:891-909.

101. Conrad WAJIToBE. Pressure-flow relationships in collapsible tubes. 1969:284-95.

102. Noordergraaf A. Circulatory system dynamics. New York: Academic P.; 1978.

103. Galford JE, McElhaney JH. A viscoelastic study of scalp, brain, and dura. Journal of biomechanics 1970;3:211-21.

104. Aaslid R, Newell DW, Stooss R, Sorteberg W, Lindegaard KF. Assessment of cerebral autoregulation dynamics from simultaneous arterial and venous transcranial Doppler recordings in humans. Stroke 1991;22:1148-54.

105. Carmelo A, Ficola A, Fravolini ML, La Cava M, Maira G, Mangiola A. ICP and CBF regulation: a new hypothesis to explain the "windkessel" phenomenon. Acta neurochirurgica Supplement 2002;81:112-6.

106. Bhadelia RA, Bogdan AR, Wolpert SM. Cerebrospinal fluid flow waveforms: effect of altered cranial venous outflow. A phase-contrast MR flow imaging study. Neuroradiology 1998;40:283-92.

107. Anile C, Portnoy HD, Branch C. Intracranial compliance is time-dependent. Neurosurgery 1987;20:389-95.

108. Piper IR, Chan KH, Whittle IR, Miller JD. An experimental study of cerebrovascular resistance, pressure transmission, and craniospinal compliance. Neurosurgery 1993;32:805-15; discussion 15-6.

109. Avezaat CJ, van Eijndhoven JH. Clinical observations on the relationship between cerebrospinal fluid pulse pressure and intracranial pressure. Acta neurochirurgica 1986;79:13-29.

110. Tain RW, Alperin N. Intracranial pressure dynamics are not linked to aqueductal cerebrospinal fluid stroke volume. Journal of applied physiology (Bethesda, Md : 1985) 2013;114:1645.

111. Carrera E, Kim DJ, Castellani G, et al. What shapes pulse amplitude of intracranial pressure? Journal of neurotrauma 2010;27:317-24.

112. Egnor M, Rosiello A, Zheng L. A model of intracranial pulsations. Pediatric neurosurgery 2001;35:284-98.

113. van Eijndhoven JH, Avezaat CJ. Cerebrospinal fluid pulse pressure and the pulsatile variation in cerebral blood volume: an experimental study in dogs. Neurosurgery 1986;19:507-22.

114. Czosnyka M, Pickard JD. Monitoring and interpretation of intracranial pressure. Journal of neurology, neurosurgery, and psychiatry 2004;75:813-21.

115. Chan KH, Miller JD, Dearden NM, Andrews PJ, Midgley S. The effect of changes in cerebral perfusion pressure upon middle cerebral artery blood flow velocity and jugular bulb venous oxygen saturation after severe brain injury. Journal of neurosurgery 1992;77:55-61.

116. Czosnyka M, Richards HK, Whitehouse HE, Pickard JD. Relationship between transcranial Doppler-determined pulsatility index and cerebrovascular resistance: an experimental study. Journal of neurosurgery 1996;84:79-84.

117. ElSankari S, Baledent O, van Pesch V, Sindic C, de Broqueville Q, Duprez T. Concomitant analysis of arterial, venous, and CSF flows using phase-contrast MRI: a quantitative comparison between MS patients and healthy controls. Journal of cerebral blood flow and metabolism : official journal of the International Society of Cerebral Blood Flow and Metabolism 2013;33:1314-21.

118. Carney N, Totten AM, O'Reilly C, et al. Guidelines for the Management of Severe Traumatic Brain Injury, Fourth Edition. Neurosurgery 2017;80:6-15.

119. Helbok R, Olson DM, Le Roux PD, Vespa P. Intracranial pressure and cerebral perfusion pressure monitoring in non-TBI patients: special considerations. Neurocritical care 2014;21 Suppl 2:S85-94.

120. Daouk J, Bouzerar R, Baledent O. Heart rate and respiration influence on macroscopic blood and CSF flows. Acta radiologica (Stockholm, Sweden : 1987) 2017;58:977-82.

Mårten Unnerbäck graduated from medical school at Lund University 2002. After two years of internship in Kiruna he returned to the south of Sweden and became an anaesthesiologist. He works as a consultant in Intensive Care Medicine at Skåne University Hospital, sharing his time between clinical work, education and research.

FACULTY OF
MEDICINE

LUND
UNIVERSITY